

Impact of changes in climate and CO₂ on the carbon storage potential of vegetation under limited water availability using SEIB-DGVM version 3.02

Shanlin Tong^{1,2,3}, Weiguang Wang^{2,3*}, Jie Chen^{1*}, Chong-Yu Xu⁴, Hisashi Sato⁵, Guoqing Wang⁶

¹State Key Laboratory of Water Resources and Hydropower Engineering Science, Wuhan University, Wuhan, 430072, Peoples R China

²State Key Laboratory of Hydrology-Water Resources and Hydraulic Engineering, Hohai University, Nanjing, 210098, Peoples R China

³College of Hydrology and Water Resources, Hohai University, Nanjing, 210098, Peoples R China

⁴Department of Geosciences, University of Oslo, Oslo, N-0316, Norway

⁵Japan Agency for Marine-Earth Science and Technology, Yokohama, 236-0001, Japan

⁶Nanjing Hydraulic Research Institute, Nanjing, 210029, Peoples R China

*Correspondence to: Weiguang Wang (wangweiguang2016@126.com); Jie Chen (jiechen@whu.edu.cn)

Abstract

Documenting year-to-year variations in carbon storage potential in terrestrial ecosystems is crucial for the determination of carbon dioxide (CO₂) emissions. However, the magnitude, pattern and inner biomass partitioning of carbon storage potential, and the effect of the changes in climate and CO₂ on inner carbon stocks, remain poorly quantified. Herein, we use a spatially explicit individual based-dynamic global vegetation model to investigate the influences of the changes in climate and CO₂ on the enhanced carbon storage potential of vegetation. The modelling included a series of factorial simulations using the CRU dataset from 1916 to 2015. The results show that CO₂ predominantly leads to a persistent and widespread increase in light-gathering vegetation biomass carbon stocks (GVBC) and water-gathering vegetation biomass carbon stocks (WVBC). Climate change appears to play a secondary role in carbon storage potential. Importantly, with the intensification of water stress, the magnitude of the light- and water-gathering responses in vegetation carbon stocks gradually decreases. Plants adjust carbon allocation to decrease the ratio between GVBC and WVBC for capturing more water. Changes in the pattern of vegetation carbon storage was linked to zonal limitations in water, which directly weakens and indirectly regulates the response of potential vegetation carbon stocks to a changing environment. Our findings differ from previous modelling evaluations of vegetation that ignored inner carbon dynamics and

32 demonstrates that the long-term trend in increased vegetation biomass carbon stocks is driven by CO₂
33 fertilization and temperature effects that are controlled by water limitations.

34 **1 Introduction**

35 As a result of the changes in climate and atmospheric carbon dioxide (CO₂), the terrestrial ecosystem
36 carbon cycle exhibits remarkable trends in interannual variations, which induce uncertainty in estimated
37 carbon budgets (Erb et al., 2018; Keenan et al., 2017). Recent studies assessing interannual fluctuations
38 in terrestrial carbon sinks have shown that the land carbon cycle is the most uncertain component of the
39 global carbon budget (Ahlstrom et al., 2015; Piao et al., 2020; Jung et al., 2017; Humphrey et al., 2018;
40 Gentine et al., 2019; Humphrey et al., 2021). These uncertainties result from an incomplete understanding
41 of vegetation biomass carbon production, allocation, storage, loss, and turnover time (Bloom et al., 2016).
42 The extent and distribution of vegetation carbon storage is central to our understanding of how to
43 maintain a balanced land carbon cycle. Changes in terrestrial vegetation carbon storage have a significant
44 effect on atmospheric CO₂ concentrations and determine whether biomes become a source or sink of
45 carbon (Erb et al., 2018; Humphrey et al., 2018; Terrer et al., 2021). Therefore, investigating the
46 processes producing changes in carbon storage is key to improving the accuracy of estimated terrestrial
47 carbon budgets, and to tap the greenhouse-gas moderation potentials of vegetation (Ipcc, 2007; Roy et
48 al., 2001).

49

50 The atmospheric CO₂ concentration are affected by the vegetation carbon stock, while the long-term
51 trend of vegetation carbon storage capacity is also affected by the changes in climate and CO₂. Since the
52 beginning of industrialization, there has been a noticeable enhancement in the capacity of storing and
53 sequestering carbon, which is needed for stabilizing greenhouse gas concentrations and mitigating global
54 warming (Chen et al., 2019; Pan et al., 2011; Le Noë et al., 2020; Magerl et al., 2019; Bayer et al., 2015;
55 Harper et al., 2018). Due to the interaction between terrestrial vegetation and a changing environment,
56 both photosynthesis and respiration of the vegetation also changed. To better absorb CO₂ and sunlight
57 required for photosynthesis, vegetated zones are gradually covered by vegetation with higher plant height
58 and wider leaf area. This change has coincided with a widespread change in other vegetation features,
59 including a positive increase in annual gross primary productivity and a greening of the biosphere

60 (Madani et al., 2020; Zhu et al., 2016). The spatiotemporal distribution and environmental drivers in total
61 carbon storage potential have been well documented on the basis of model estimates and satellite-based
62 assessments (Erb et al., 2007; Erb et al., 2018; Bazilevich et al., 1971; Saugier et al., 2001; Bartholome
63 and Belward, 2005; Olson et al., 1983; Pan et al., 2013; Ajtay et al., 1979; Ruesch and Gibbs, 2008;
64 Kaplan et al., 2011; Shevliakova et al., 2009; Prentice et al., 2011; West et al., 2010; Hurtt et al., 2011).
65 In contrast, the variability of inner components of carbon storage potential has not been extensively
66 studied. Without an accurate assessment of the dynamics of each fraction, attribution of carbon storage
67 potential to environmental drivers is highly uncertain. Consequently, partitioning potential vegetation
68 carbon storage and revealing its inner processes are essential to accurately comprehend the current state
69 of carbon storage capacity and reveal the influence of various drivers on the long-term trend of carbon
70 storage potential.

71

72 The change of carbon storages in vegetation inner components is not only affected by environmental
73 factors, but also controlled by allocation scheme of assimilated carbon. Fractional dynamics of the carbon
74 stock are widely used as a key indicator to investigate the responses of vegetation to environmental
75 drivers, which also reflect the response strategies of vegetation in environments with different water
76 limitations (Yang et al., 2010). In arid region, vegetation utilizes a tolerance strategy to allocate biomass,
77 storing more biomass carbon in roots to resist enhanced water stress (Chen et al., 2013). Conforming to
78 the optimal partitioning hypothesis, plants store more carbon in shoots and leaves in environments where
79 water is more available and shift more carbon to roots when water is more limited (Yang et al., 2010;
80 McConnaughay and Coleman, 1999). Water availability controls both carbon allocation and storage and
81 can potentially transform zones characterized by a positive response to changes in climate and CO₂ to
82 zones exhibiting a negative response. For example, global warming stimulates plant productivity,
83 Madani et al. (2020) found that there is a dramatically downward trend in the tropical productivity. With
84 increased warming, water limitations are predictable to increasingly reduce the proportion of leaves'
85 biomass, and decrease plant photosynthesis (Ma et al., 2021). Water limitations have a strong regulating
86 effect on the spatial pattern of change in vegetation carbon storage, demonstrating the effects of the
87 changes in climate and CO₂ on the dynamics of the plant organs are affected by the terrestrial water
88 gradient. Thus, it is important to systematically investigate the distinct responses of carbon storage

89 potential to changes in climate and CO₂ under differing conditions of water stress.

90

91 As documented above, many studies have investigated the total changes in zonal and global terrestrial
92 storage of carbon, while few studies have examined trends in the components partitioning of vegetation
93 carbon storage. Large gaps in our knowledge of the effects of various drivers on the partitioning of carbon
94 stocks in vegetation biomass remain. Meanwhile, plants adjust carbon allocation scheme to adapt to
95 environmental change. With increased warming, an increase in the magnitude of water stress may
96 dramatically change or even reverse the impact of these drivers on inner components of carbon storage
97 (Ma et al., 2021). Evaluating the response pattern of carbon stocks to various drivers under conditions of
98 limited water is elemental for clearly documenting the response mechanism of vegetation carbon storage
99 potential.

100

101 Here, we use a spatially explicit individual-based dynamic global vegetation model (SEIB-DGVM),
102 along with the components partitioning method to (1) systematically determine the long-term variability
103 of carbon storage potential and understand its response mechanisms, and (2) estimate trends in
104 partitioning of potential biomass carbon stocks of vegetation biomass. Throughout this study, the
105 potential biomass carbon stock, biomass carbon stored in vegetation without anthropogenic disturbance,
106 is recognized as a proxy for the potential of carbon storage by natural vegetation. Using a set of factorial
107 simulations to isolate responses to environmental change, we analyse the contributions of multiple
108 driving factors to the trends of two fractions of carbon stock at large scales individually. We then
109 conceptualize the role of water availability through an aridity index (AI), in which hydrological zones
110 are subdivided by their degree of aridity. By comparing the differences in the magnitude of response
111 between the fractions of light- and water-gathering carbon stocks for varying degrees of water availability,
112 we assess the effect of water limitations on the response pattern of potential carbon stocks to changes in
113 climate and CO₂.

114 **2 Model description, experimental design, observational data, and evaluation metrics**

115 In this section, we provided a list of data source (Sect. 2.1), an overview of the modelling concept (Sect.
116 2.2), the representation of biomass carbon stock partitioning in the SEIB-DGVM (Sect. 2.3), an overview

117 of the experimental scheme used in the model simulations (Sect. 2.4), and an overview about data source
118 and pre-processing of observation dataset for model evaluation (Sect. 2.5).

119 **2.1 Forcing Data**

120 Long-term daily meteorological time-series data are required to run model simulations, including
121 precipitation, daily range of air temperature, mean daily air temperature, downward shortwave radiation
122 at midday, downward longwave radiation at midday, wind velocity and relative humidity. These data
123 were obtained from the Climatic Research Unit (CRU) time series 4.00 gridded dataset (degree 0.5°) for
124 the period 1901–2015 (Harris et al., 2020). Because the CRU dataset is a monthly based dataset, the
125 monthly meteorological data were converted into daily climatic variables by supplementing daily
126 climatic variability within each month using the National Centre for Environmental Prediction (NCEP)
127 daily climate dataset. The NCEP data, displayed using the T62 Gaussian grid with 192×94 points, was
128 interpolated into a 0.5° grid (which corresponds to the CRU dataset) using a linearly interpolation method.
129 By combining the CRU data, with the interpolated NCEP dataset, we were able to directly obtain the
130 most of driving meteorological data (details in Sato et al. (2020)). Neither the CRU nor NCEP datasets
131 included downward shortwave and longwave radiation at midday. Thus, daily cloudiness values in the
132 NCEP were used to calculate radiation values using empirical functions (Sato et al., 2007). These data
133 were all aggregated to a daily timescale with 0.5° resolution to run SEIB-DGVM.

134

135 Atmospheric CO_2 concentrations were collected from Sato et al. (2020), which contains reconstructed
136 CO_2 concentrations between 1901 and 2015. The statistical reconstruction of global atmospheric CO_2
137 was used in this analysis. These reconstructions were based on present annual CO_2 concentrations
138 recorded from the Mauna Loa monitoring station. These data assume atmospheric CO_2 concentration
139 was 284 ppm in 1750, and statistically interpolates atmospheric CO_2 concentrations to fill the gap from
140 1750 to 2015.

141

142 The physical parameters of the soil used in the model include soil moisture at the saturation point, field
143 capacity, matrix potential, wilting point and albedo. These data were obtained from the Global Soil
144 Wetness Project 2.

145 **2.2 Overview of modelling concept in SEIB-DGVM**

146 Model SEIB-DGVM version 3.02 (Sato et al., 2020) was employed in this study. This is a process-based
147 dynamic global vegetation model driven by meteorological and soil data. It is an explicit and
148 computationally efficient carbon cycle model designed to simulate transient effects of environmental
149 change on terrestrial ecosystems and land-atmosphere interactions. It describes three groups of processes:
150 land-based physical processes (e.g., hydrology, radiation, aridity), plant physiological processes (e.g.,
151 photosynthesis, respiration, litter), and plant dynamic processes (e.g., establishment, growth, mortality).
152 Twelve plant functional types (PFTs) were classified. During the simulation, a sample plot was
153 established at each grid box, and then the growth, competition, and mortality of each the individual PFTs
154 within each plot were modelled by considering the specify conditions for that individual as it relates to
155 other individuals that surround it (Sato et al., 2007).

156

157 SEIB-DGVM treats the relationships between soil, atmosphere, and terrestrial biomes in a consistent
158 manner, including the fluxes of energy, water, and carbon. Based on specified climatic conditions and
159 soil properties, SEIB-DGVM simulates the carbon cycle, energy balance, and hydrological processes.
160 SEIB-DGVM utilizes three computational time steps: (1) During the growth phase, the metabolic
161 procedures including photosynthesis, respiration, and carbon allocation are executed for each individual
162 tree every simulation day. (2) The monthly process of tree growth including reproduction, trunk growth,
163 and expansion of a cross-sectional area of the crown are executed. (3) On the last day of each year, the
164 height of the lowest branch increases as a result of purging crown disks, or self pruning of branches, at
165 the bottom of the crown layer. The simulated unit of the model is a 30 m × 30 m spatially explicit ‘virtual
166 forest’. A grass layer was placed under the woody layer, and provides for a comprehensive, spatially
167 explicit quantification of terrestrial carbon sinks and sources. The soil depth was set at 2 m and was
168 divided into 20 layers, each with a thickness of 0.1 m. The photosynthetic rate of a single-leaf was
169 simulated following a Michaelis-type function (Ryan, 1991). Respiration was divided into two types:
170 growth respiration and maintenance respiration. Growth respiration is defined as a construction cost for
171 plant biosynthesis, which is quantified by the chemical composition of each organ (Poorter, 1994).
172 Maintenance respiration of live plants occurs every day regardless of the phenological phase, and is
173 controlled by the temperature and nitrate content of each organ (Ryan, 1991). For a wide variety of plant

174 organs, the maintenance respiration rate is linearly related to the nitrogen content of living tissue. The
 175 relative proportions of nitrogen in each organ for any PFT are linearly correlated. N-deposition doesn't
 176 include in SEIB-DGVM. Atmospheric CO₂ was envisioned to be absorbed by photosynthesis of woody
 177 PFTs and grass PFTs. This assimilated carbon flux was then allocated into all the plant organs (leaf,
 178 trunk, root, and stock), where maintenance respiration and growth respiration occur. The hydrology
 179 module treats precipitation, canopy interception, transpiration, evaporation, meltwater, and penetration.

180 **2.3 Carbon stock of vegetation biomass partitioning**

181 **2.3.1 Parameterization of daily allocation**

182 Flexible allocation schemes about resources and biomass are set up in the framework of the SEIB-DGVM
 183 biogeochemical model. Based on the updated observation data, the allocation schemes of Boreal Needle-
 184 leaved summer-green trees and Tropical Broad-leaved evergreen trees were improved at SEIB-DGVM
 185 V3.02. Allocation schemes of other PFTs are the same as the original version. Atmospheric CO₂ is
 186 assimilated by the photosynthesis of both woody and grass foliage, and then is added into the non-
 187 structural carbon of the plant. This non-structural carbon of photosynthetic production is allocated to all
 188 the plant organs (foliage, trunk, root, and stock), supplying what is needed for the maintenance and
 189 growth of each organ. When the non-structural carbon is greater than 0 during the growth phase, the
 190 following dynamic carbon allocation is executed for each individual plant at the daily time scale, such
 191 that:

192 (1) When the fine root biomass ($mass_{root}$) of wood or grass does not satisfy minimum requirements for
 193 fulfilling functional balance ($mass_{leaf}/FR_{ratio}$), the mass of non-structural carbon is allocated to the root
 194 biomass to supplement the deficit. Here, $mass_{leaf}$ is the leaf biomass, and FR_{ratio} is the ratio of $mass_{leaf}$ to
 195 $mass_{root}$ satisfying the functional balance.

196 (2) The stock biomass is supplemented until it is equal to leaf biomass. This scheme is active after the
 197 first thirty days of the growing phase.

198 (3) Woody leaf biomass is constrained by three limitations of the maximum leaf biomass, which are
 199 calculated as follows:

$$200 \quad max_1 = (crown_{area} + \pi crown_{diameter} crown_{depth}) \frac{LA_{max}}{SLA} \quad (1)$$

$$201 \quad max_2 = ALM_1 \frac{\pi(dbh_{heartwood}/2 + dbh_{sapwood}/2)^2 - \pi(dbg_{heartwood}/2)^2}{SLA} \quad (2)$$

202 $max_3 = \frac{mass_{available}}{RG_f}$ (3)

203 $mass_{leaf} = \min(max_1, max_2, max_3)$ (4)

204 where max_1 , max_2 , and max_3 are, respectively, maximum leaf biomass for a given crown surface
 205 area, cross-sectional area of sapwood, and non-structural carbon; SLA is a constant of PFTs leaf area
 206 ($m^2 g^{-1}$); LA_{max} is the plant functional type specific maximum leaf area per unit crown surface area
 207 excluding the bottom soffit ($m^2 m^{-2}$); ALM_1 represents the area of transport tissue per unit biomass, and
 208 is a constant (dimensionless). If the $mass_{leaf}$ is less than the minimum (max_1, max_2, max_3), the mass of
 209 non-structural carbon is allocated into leaf biomass to supplement the deficit.

210 When the leaf area index of grass equals the optimal leaf area index, it stops to allocate non-structural
 211 carbon to grass leaf, which is calculated as:

212 $lai_{opt} = \frac{\ln par_{grass} - \ln \left(\frac{p_{sat}}{lue} \left[\left(1 - \frac{cost/SLA}{0.09093 \times dlen \times p_{sat}} \right)^{-2} - 1 \right] \right)}{eK}$ (5)

213 where lai_{opt} is the optimal leaf area index ($m^2 m^{-2}$); par_{grass} is the grass photosynthetically active
 214 radiation ($\mu mol \text{ photon } m^{-2} s^{-1}$); p_{sat} is the light-saturated photosynthetic rate ($\mu CO_2 m^{-2} s^{-1}$); lue is
 215 the light-use efficiency of photosynthesis ($mol CO_2 mol \text{ photon}^{-1}$); $cost$ is the cost of maintaining
 216 leaves per unit leaf mass per day ($g DM g DM^{-1} day^{-1}$); $dlen$ is day length (hour); and eK is light
 217 attenuation coefficient at midday.

218 (4) When non-structural carbon is less than 10 g dry mass (DM) PFT⁻¹ or annual NPP is less than 10 g
 219 DM PFT⁻¹ in the previous year, the following daily simulation processes (5-6) will be skipped.

220 (5) When total woody biomass is more than 10 kg DM, which defines the minimum tree size for
 221 reproduction. This 10% NSC is used for every daily process of reproduction, including having flowers,
 222 pollen, nectar, fruits, and seeds.

223 (6) During the simulation of trunk growth, the remaining non-structural carbon is allocated to sapwood
 224 biomass. There is no direct allocation to heartwood, which is transformed slowly from sapwood biomass.
 225 For grass PFTs biomass, the densities of all organs comprising the biomass never decline below 0.1 g
 226 DM m⁻² even if the environment is deteriorated for grass survival. A more detailed description of SEIB-
 227 DGVM is given by Sato et al. (2007).

228

229 To control plant phenology and the rate of photosynthesis as a function of the limitation in terrestrial
 230 water, the physiological status of the limitation of terrestrial water is calculated as:

231 $p_{sat} = PMAXce_{tmp}ce_{co_2}ce_{water}$ (6)

232 $ce_{water} = \sqrt{stat_{water}}$ (7)

233 $stat_{water} = \frac{\max(pool_{w(1)}/Depth_{(1)}, pool_{w(2)}/Depth_{(2)}) - W_{wilt}}{W_{fi} - W_{wilt}}$ (8)

234 where p_{sat} is the single-leaf photosynthetic rate of tree PFTs and grass PFTs ($\mu\text{mol CO}_2 \text{ m}^{-2} \text{ s}^{-1}$);
 235 $PMAX$ is the potential maximum of photosynthetic rate ($\mu\text{mol mol}^{-1} \text{ CO}_2 \text{ m}^{-2} \text{ s}^{-1}$); ce_{tmp} and ce_{co_2} are
 236 the temperature and CO_2 concentration effect coefficient (dimensionless), separately; ce_{water} is the
 237 water effect coefficient (dimensionless); $stat_{water}$ is the physiological status of the terrestrial water
 238 limitation, which ranges between 0.0–1.0, dimensionless; $pool_{w(n)}$ is the water content in soil layer n,
 239 mm; $Depth_{(n)}$ is the depth of the soil layer n, mm; W_{wilt} is soil moisture at the wilting point, m m^{-1} ;
 240 and W_{fi} is soil moisture at field capacity, m m^{-1} . When the temperature of all soil layers is less than 0°
 241 C, $stat_{water}$ is equal to 0.

242 2.3.2 Carbon stock partitioning method

243 SEIB-DGVM allocates and stores the biomass carbon in four pools of woody PFT (foliage, trunk, root,
 244 and stock) and three pools of grass PFT (foliage, root, and stock). To investigate the fractional variability
 245 of carbon sequestration potential between the pools, we partitioned potential vegetation carbon stocks
 246 based on the physiological function of the plant (Figure A1). The root-shoot ratio (R/S) has been used to
 247 distinguish and investigate the ratio of below-ground biomass (root biomass) and above-ground biomass
 248 (shoot biomass) (Zhang et al., 2016). In this study, we adjusted the method of calculating the R/S ratio
 249 by distinguishing between the light-gathering vegetation biomass carbon stock (LVBC) and the water-
 250 gathering vegetation biomass carbon stock (WVBC). LVBC represents the biomass carbon invested by
 251 plant is used to gather sunlight, including biomass carbon from woody foliage, woody trunk, and grass
 252 foliage. WVBC represents biomass carbon used to gather water, including biomass carbon from woody
 253 fine roots and grass fine roots, excluding the stock pool. Stock biomass is used for foliation after dormant
 254 phase and after fires in PFTs, which is reserve resource in each individual tree. Fine root biomass is just
 255 a tiny fraction to the total biomass, but is has a very high turnover rate and determines the capacity of
 256 vegetation to absorb soil water. Thus,

257 $\frac{GVBC}{WVBC} = \frac{W_{massleaf} + W_{masstrunk} + G_{massleaf}}{W_{massroot} + G_{massroot}} \times 100\%$ (9)

258 where $GVBC$ is aboveground vegetation biomass carbon stock (kg C m^{-2}); $WVBC$ is belowground

259 vegetation biomass carbon stock (kg C m^{-2}); $W_{mass_{leaf}}$ is the leaf biomass carbon stock of wood (kg
 260 C m^{-2}); and $W_{mass_{trunk}}$ is the trunk biomass carbon stock of wood (kg C m^{-2}), including both branch
 261 and structural roots. This biomass is simplistically attributed to aboveground organs and is used primarily
 262 to support the plant. $G_{mass_{leaf}}$ is the leaf biomass carbon stock of grass (kg C m^{-2}); whereas
 263 $W_{mass_{root}}$ and $G_{mass_{root}}$ are functional root (fine roots) biomass carbon stocks of wood and grass,
 264 separately (kg C m^{-2}), which absorb water and nutrition from soil.

265 2.4 Experimental design

266 2.4.1 Setup of model runs

267 SEIB-DGVM simulations begin with seeds of selected PFTs planted in bare ground. The establishment
 268 of PFTs seeds are determined by the climatic conditions in each grid cell. We inputted the transient
 269 climate data from 1901 to 1915 to spin up the model in a repetitive loop. No obvious trend in climatic
 270 factors was observed during this period (Tei et al., 2017). A spin-up period of 1050 years was necessary
 271 to bring the terrestrial vegetation carbon cycle into a dynamic equilibrium. To reach quasi-equilibrium
 272 in the vegetation biomass, about 1000 years of simulation was required as a spin-up procedure.

273 2.4.2 Factorial simulation scheme

Table 1. List of factorial simulations used in this study

Factorial simulation	CO ₂ concentration	Precipitation	Temperature	Radiation	Other drivers
S1	√	√	√	√	√
S2	√				
S3	√	√			
S4	√		√		
S5	√			√	
S6	√				√

Note: In factorial simulation S1, historical atmospheric CO₂ concentration and historical climate fields from the CRU data set were used. In simulation S2, only historical atmospheric CO₂ concentration was used, and climate variables of the transient period (1901–1915) were repeatedly input. In simulation S3 (or S4, S5), only historical atmospheric CO₂ concentrations and precipitation (or temperature, radiation) were input, and climate variables of the transient period (1901–1915) were repeatedly input. In the last simulation S6, historical atmospheric CO₂ concentrations and other climate variables were input, including wind velocity and relative humidity.

274 In order to further quantify the relative contributions of varying atmospheric CO₂ concentrations,
 275 precipitation, temperature, radiation, and other factors, we performed six factorial simulations. Other

276 factors included wind velocity and relative humidity, which had remarkable effects on the change in
277 vegetation carbon stock at zonal scale. In simulation S1, atmospheric CO₂ concentration and all of
278 climate variables were varied. In simulation S2, only atmospheric CO₂ concentration was varied, and
279 climate variables were held constant (Climate variables of the transient period (1901-1915) were
280 repeatedly inputted). In simulation S3 (or S4, S5), atmospheric CO₂ and precipitation (or temperature,
281 radiation) were varied, and other climate variables were held constant. In simulation S6, atmospheric
282 CO₂, wind velocity, and relative humidity were varied, and other climate variables were held constant.
283 Finally, S2 was used to evaluate the effects of CO₂ fertilization on carbon stock variation. The differences
284 of S2-S3, S2-S4, S2-S5, and S2-S6 were used to evaluate the response of carbon stock growth to
285 precipitation, temperature, radiation, and other drivers, respectively.

286 **2.4.3 Non-parametric test methods**

287 Each driving factor (atmosphere CO₂, precipitation, temperature, and radiation) has a different influence
288 on the carbon stock, so it is difficult to make a simple pre-assumption about the population distribution
289 pattern for factorial simulations. We used the non-parametric Mann-Kendall and Sen's slope estimator
290 statistical tests (Gocic and Trajkovic, 2013) to assess the ability of SEIB-DGVM to simulate the response
291 patterns of carbon storage potential to a change in climate and CO₂ concentrations. We regressed the
292 simulated hundred-year mean global average carbon stock time series to reveal the accumulative
293 influences of the single variables based on the factorial simulations where only one or two drivers were
294 varied. As shown in Figures A2, 3, detection trends of LVBC and WVBC for all driving factors
295 performed statistically well (in agreement at the 95% confidence intervals), indicating this analytical
296 method was suitable for trend attribution at the global scale.

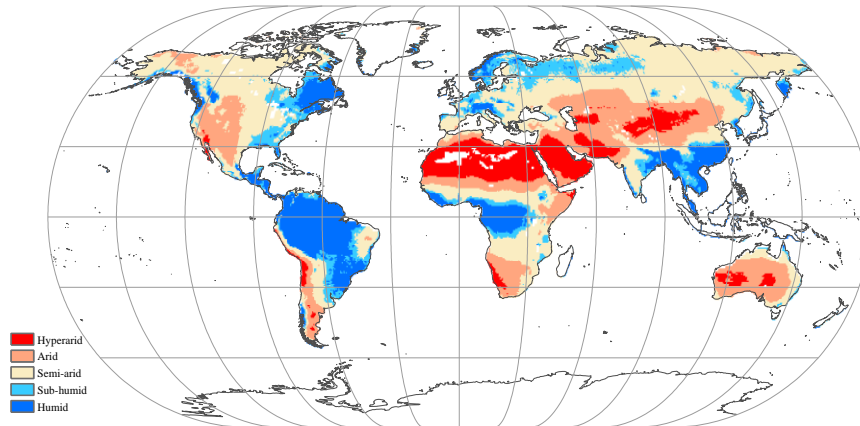


Figure 1. Global spatial patterns of water availability. Spatial variations in water availability were categorized based on a 115-year average aridity index (AI), defined as the ratio of the multiyear mean precipitation to the potential evapotranspiration. Categories include: hyper-arid ($AI \leq 0.05$), arid ($0.05 < AI \leq 0.2$), semi-arid ($0.2 < AI \leq 0.5$), sub-humid ($0.5 < AI \leq 0.65$), and humid ($AI > 0.65$).

298 Locally available water strongly regulates and limits the response of carbon stocks to changes in climate
 299 and CO_2 . We used aridity index (AI) to distinguish between the global hydrological regions for
 300 comparing the long-term trend in carbon stocks over different hydrological environments, and for
 301 quantifying the influences of each hydrological environment on the variations in the trends. The AI was
 302 defined as:

$$303 \quad AI = \frac{\bar{P}}{\overline{ET_p}} \quad (10)$$

304 where \bar{P} is the multiyear mean precipitation ($mm \text{ year}^{-1}$); and $\overline{ET_p}$ is the multiyear mean potential
 305 evapotranspiration ($mm \text{ year}^{-1}$), which was calculated by the Penman-Monteith model (Monteith and
 306 Unsworth, 1990). As in a previous study (Chen et al., 2019), five hydrological regions (Figure 1) were
 307 categorized based on a 115-year average AI (1901–2015): including a hyper-arid region ($AI \leq 0.05$),
 308 arid region ($0.05 < AI \leq 0.2$), semi-arid region ($0.2 < AI \leq 0.5$), sub-humid region ($0.5 < AI \leq 0.65$), and
 309 humid region ($AI > 0.65$).

310 **2.5 Observation dataset for model evaluation**

311 A global time series of potential vegetation carbon was modelled by the SEIB-DGVM between 1916-
 312 2015. In terrestrial vegetation biomes, there is a high correlation between biomass carbon stock density
 313 and NPP per unit (Erb et al., 2016; Kindermann et al., 2008) (Figure A1). Thus, we collected NPP

314 observation dataset and used NPP as a proxy of the carbon stock to assess model accuracy. Ecosystem
315 Model-Data Intercomparison (EMDI) builds upon the accomplishments of the original worldwide
316 synthesis of NPP measurements and associated model driver data prepared by Global Primary Production
317 Data Initiative. We obtained the monitoring station data from the EMDI working group, and then
318 compared their data with modelled multiyear average NPP in the period of 1916-1999 (Figure 2).

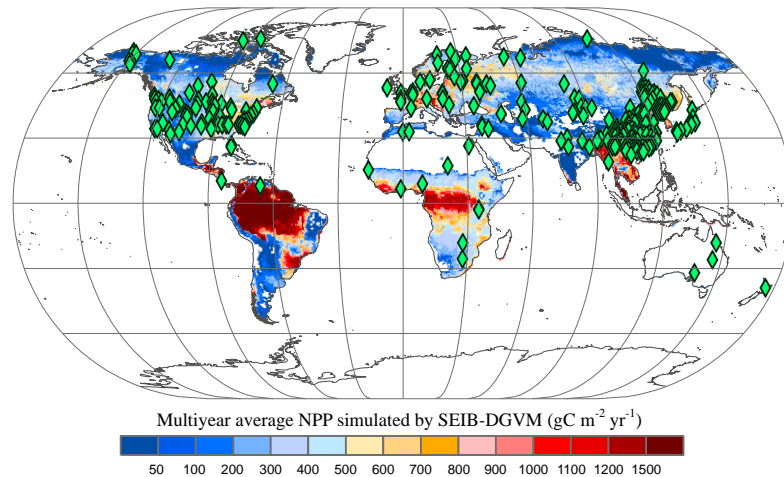


Figure 2. Multiyear average NPP simulated by SEIB-DGVM and EMDI global site distribution.

Green rhombuses indicate the monitoring stations of the EMDI.

319 However, *in-situ* observations are sparse for global spatial-temporal validation. Therefore, we used the
320 MOD17A3 products to further verify the simulated potential NPP in the twenty first century. These data
321 were collected by the Moderate Resolution Imaging Spectroradiometer and are some of the most widely
322 used data to assess the accuracy of global model simulations (Gulbeyaz et al., 2018). The natural
323 vegetation zones refer to the hypothetical condition that would prevail in an assumed absence of
324 anthropogenic activity, but under historical climate fields (Erb et al., 2018; Haberl et al., 2014). The
325 potential NPP is defined as that assimilated carbon stored in natural vegetation without the disturbance
326 of anthropogenic activities (Erb et al., 2018).

327 In order to distinguish the distribution of vegetation zones without anthropogenic disturbance, we
328 obtained global land cover types in the period 2001-2015 from MCD12C1 (Table A1). It was defined as
329 vegetation grid that the land cover type of this grid is evergreen needleleaf forest, evergreen broadleaf
330 forest, deciduous needleleaf forest, deciduous broadleaf forest, mixed forest, closed shrublands, open
331 shrublands, woody savannas, savannas or grasslands. Grid covered by other 7 land types was defined as
332 non-vegetation grid. Then, we calculated the proportion of each land cover types in corresponding 0.5°

333 grid unit. The land cover type of grid unit was determined by the max proportion among 17 land cover
334 types. Part of grids covered by grassland were grazed by livestock, leading to the decrease of NPP of
335 grass PFTs. We obtained land-use forcing data from Land-Use Harmonization (LUH2) to map the
336 distribution of managed pasture data from 2001 to 2015 (Hurt et al., 2020). As shown in Figure A4,
337 grassland in eastern Asia, western Europe, south central Africa, and western South America were
338 severely affected by grazing. To exhibit the disturbance of managed pasture, we calculated the mean
339 fraction of managed pasture within the corresponding 0.5° grid unit. When the fraction of managed
340 pasture over 0.01, the grid covered by grassland was considered to be affected by managed pasture. We
341 filtered grassland affected by pasture to map the distribution of natural vegetation zones without
342 anthropogenic disturbance (Figure A5).

343 3 Results and discussion

344 3.1 Evaluation of SEIB-DGVM

345 Figure 3 illustrates the comparison between model simulated and observed multi-year mean NPP during
346 1916-1999. The determined coefficient (R^2) between EMDI observed and estimated multiyear average
347 NPP of 669 *in-situ* observations is 0.54, which is significant at the $p=0.01$ level. The slope of the
348 regressed line is 0.70 during the twentieth century.

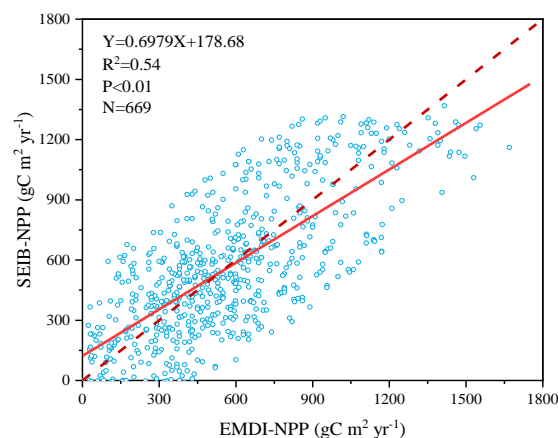


Figure 3. Comparison of multiyear average NPP calculated by SEIB-DGVM and EMDI for the twentieth century. The solid line is the best fit curve; and the dashed line represents a perfect correspondence in the results of the two.

349 Based on land cover types dataset from 2001 to 2015, we obtained NPP-MOD17A3 data in natural
350 vegetation zones without anthropogenic disturbance at the same period. Figure 4 shows that the modelled
351 NPP from the SEIB-DGVM exhibited a high degree of consistency with the NPP-MOD17A3 data in
352 natural vegetation zones over the period ($R^2=0.63$, $p<0.05$). The general spatiotemporal agreement
353 between the simulated NPP derived from SEIB-DGVM with *in-situ* observations and derived from
354 satellites reveals that it is reasonable to use the SEIB-DGVM simulations to evaluate the same
355 mechanisms controlling global potential biomass carbon stocks of vegetation.

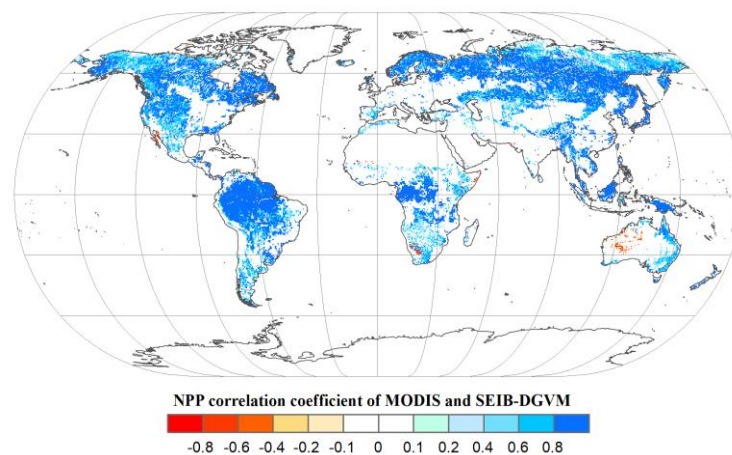


Figure 4. Spatial patterns in the potential NPP correlation coefficients between SEIB-DGVM and MODIS between 2001–2015. These data were used to validate SEIB-DGVM.

356 Finally, the modelled result of potential vegetation biomass carbon stock was compared with current
357 existing data from the literature and state-of-the-art datasets. Figure 5 shows that the modelled results are
358 within the range of potential carbon stocks, which indicate that the SEIB-DGVM reliably simulated the
359 carbon stock dynamics.

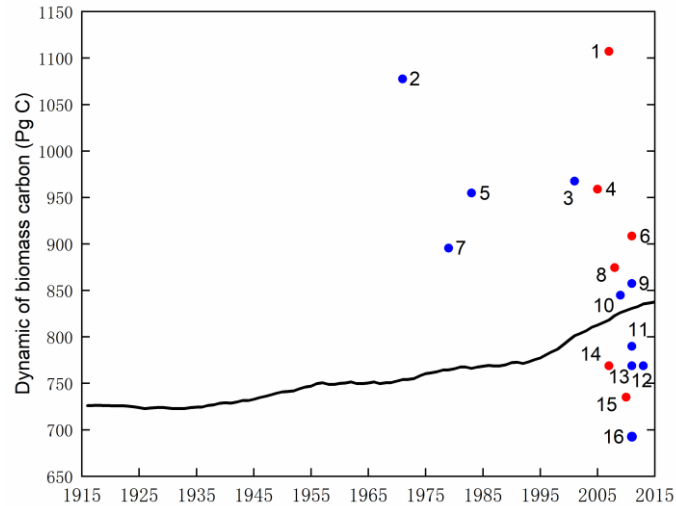


Figure 5. Estimates of the potential vegetation biomass carbon stock from the literature (blue plot), state-of-the-art datasets (red plot) and this study (black line). Datasets are from the following studies: (1)(Erb et al., 2018; Erb et al., 2007), (2)(Bazilevich et al., 1971), (3)(Saugier et al., 2001), (4)(Erb et al., 2018; Bartholome and Belward, 2005), (5)(Olson et al., 1983), (6)(Erb et al., 2018; Pan et al., 2011), (7)(Ajtay et al., 1979), (8)Erb et al., 2018; Ruesch and Gibbs, 2008), (9)(Kaplan et al., 2011), (10)(Shevliakova et al., 2009), (11)(Kaplan et al., 2011), (12)(Pan et al., 2013), (13)(Prentice et al., 2011), (14)(Erb et al., 2018; Erb et al., 2007), (15)(Erb et al., 2018; West et al., 2010), (16)(Hurt et al., 2011).

360 3.2 Enhanced carbon stocks and its fractions

361 We distinguished the changes of LVBC and WVBC from total vegetation carbon stocks. The historical
 362 temporal trends over the period are shown in Figure 6a. The potential vegetation carbon stock exhibits a
 363 net increase of 119.26 ± 2.44 Pg C in the last century (± 2.44 represents intra-annual fluctuation in carbon
 364 stock, which is the difference between maximum value and a minimum value of carbon stock within the
 365 year). Based on Pearson correlation analysis, this increasing trend of annual average carbon stock
 366 exhibits a robust agreement with the dramatic increase in atmospheric CO_2 concentration ($R^2=0.9677$,
 367 $p<0.001$), suggesting that the carbon stock is strongly affected by CO_2 fertilization. Meanwhile, the
 368 positive correlation between the carbon stock and CO_2 generally extends across LVBC ($R^2=0.9669$) and
 369 WVBC ($R^2=0.9622$). After the value of the global terrestrial carbon stock and trends were partitioned
 370 among the vegetation functional classes, we see that LVBC increases 116.18 ± 2.34 Pg C (or $\sim 15.60\%$),
 371 which explains 97.42% of total carbon stock increasing trend and dominates the positive global carbon

372 stock trend; WVBC also increases 3.08 ± 0.14 Pg C (or $\sim 18.03\%$) over the past century.

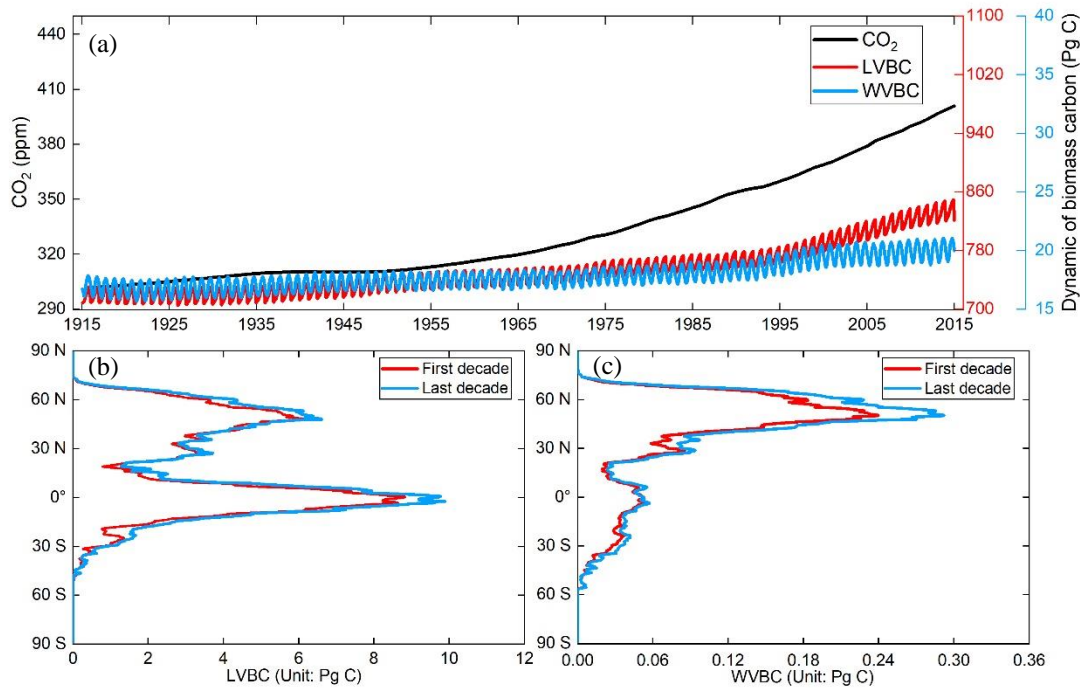


Figure 6. Global potential biomass carbon stocks of vegetation during the past 100 years. (a) The evolution of global potential biomass stocks (LVBC+WVBC), along with changes in biomass stocks that can be attributed to the variability and trend of LVBC and WVBC through the twentieth century. The red line represents the monthly value of LVBC, the blue line represents the monthly value of WVBC, and the black line represents the annual value of CO₂ concentration. **(b, c)** Zonal averaged sums of the annual LVBC and WVBC for latitudinal bands during the first decade (1916–1925, red line) and the last decade (2006–2015, blue line) shows the increased carbon stock capacity.

373 The global distributions of the decadal-average change in LVBC and WVBC are shown in Figures 6b
374 and 6c, respectively. The significant historical changes in climate and CO₂ enhance the carbon stock of
375 the terrestrial ecosystem, and their positive influences are broadly distributed across a latitudinal north–
376 south gradient. The latitudinal bands of increasing annual LVBC are mainly distributed in the tropical
377 and boreal latitudes. The decadal and inter-annual variabilities of LVBC are dominated by the tropical
378 and semi-arid zones where large portions of the zones are highly productive (Ahlstrom et al., 2015;
379 Poulter et al., 2014). Tropical LVBC dominates the long-term trend of global LVBC in the last hundred
380 years. Compared with LVBC, the increase of tropical WVBC is light. There is a single peak in the spatial
381 variation of annual WVBC (Figure 6c). WVBC exhibits robust growth at most latitudes, and increases
382 mainly in boreal latitudes.

383 **3.3 Spatial variability in estimated LVBC and WVBC trends**

384 In Figures 7(a) and 7(b), total carbon stock and LVBC exhibit a significantly increasing trend in eastern
385 South America, southern Africa, and northern Asia, while declined in central North America, northwest
386 South America, and central Africa. WVBC showed a more widely increasing tendency in North America,
387 southeastern South America, and Europe, while had a decrease trend in part zones of Asian. We find that
388 the total carbon stock as well as the light- and water-gathering vegetation biomass carbon stocks over
389 the period of 1916–2015 exhibited a remarkable spatial heterogeneity. Figure 7a shows that an increase
390 in vegetation carbon stocks occurred over zones and global aggregate levels during the entire study period.
391 About 57.39% of the terrestrial grids exhibited an increase with a noticeable trend ($p < 0.05$) in biomass
392 carbon stock; 53.82% of global grids possessed increases that were statistically significant at the $p = 0.01$
393 level. To determine the contributions of each fraction (LVBC, WVBC) to the total change in the potential
394 vegetation carbon stock, we partitioned and present the historical spatial and temporal patterns for each
395 fraction separately (Figure 7b, 7c). LVBC contributes 97.33% to the incremental change of total carbon
396 stock (116.18 ± 2.34 Pg C), with about 51.32% of the grids possessing a noticeable positive trend
397 ($p = 0.01$). Generally, spatial patterns of LVBC and the total carbon stock are consistent (Figure 7a, 7b),
398 which further supports the argument that LVBC dominates the trend in carbon stocks in most zones.
399 Although the proportion of the total change in carbon stocks is small (2.58% of total carbon stock
400 increase), about 61.00% of the land surface shows an increase in WVBC; of these terrestrial grids, 55.81%
401 was characterized by a significant $p = 0.01$ increase.

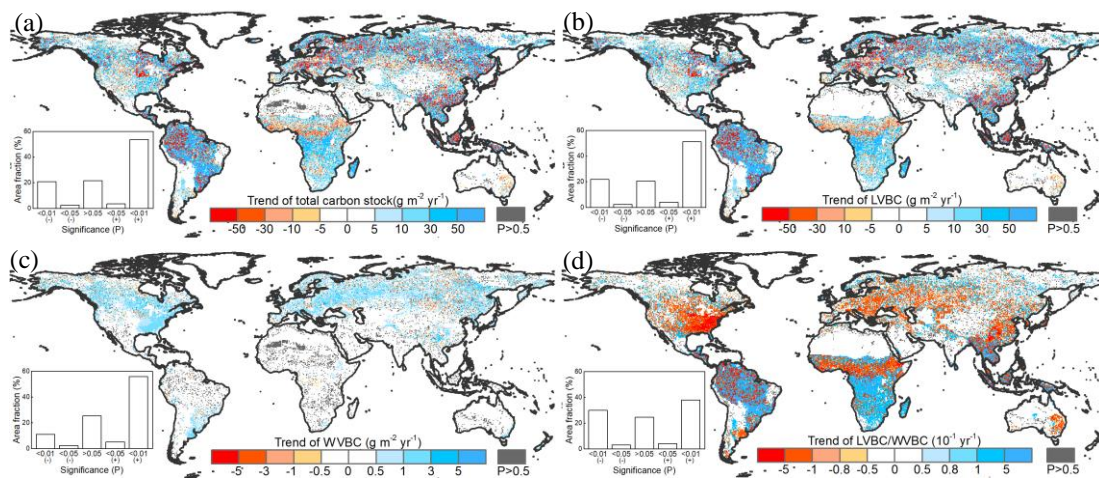


Figure 7. Spatial patterns in the trends of potential vegetation carbon stocks and their fractions

from 1916 to 2015. Difference induced by changes in climate and CO₂ in terrestrial biomass carbon stock (a), LVBC (b), and WVBC (c) during the historic period 1916–2015. The blue bar indicates the significantly increasing trends and the red bar indicates the significantly decreasing trends in carbon stocks. (d) Trend in the LVBC/WVBC ratio from 1916 to 2015. The blue bar indicates significantly increasing trends in the ratio, and vice versa. The grey bar indicates the trend is statistically insignificant ($P > 0.05$). The sub-graphs show the significant test results. A ‘+’ symbol indicates a positive trend, and vice versa.

402 Under the influences of a changing climate and CO₂ concentrations, there is a slight increase in the ratio
403 of global LVBC/WVBC; the rate of increase is 0.0171 yr^{-1} in the last hundred years, which is significant
404 at the 0.01 level (Figure 7d). About 42.08% of the terrestrial grids exhibited an increase with a noticeable
405 trend ($p < 0.05$) in the ratio of LVBC and WVBC; 37.95% of global grids possessed increases that were
406 statistically significant at the $p = 0.01$ level. Meanwhile, 33.32% of the land surface shows a significant
407 decrease in LVBC/WVBC; of these terrestrial grids, 30.06% was characterized by a significant $p = 0.01$
408 decrease. Zones with noticeable increases in the ratio of LVBC to WVBC are mainly located in southern
409 Africa, central South America, and northern Eurasia. Negative trends in LVBC/WVBC ratios are found
410 in northern America, southern Europe, and tropical Africa.

411 **3.4 Responses of LVBC and WVBC to environmental drivers**

412 The responses of LVBC and WVBC to changes in climate and CO₂ are both positive at the global level
413 (Figure 8a, 8c), although zonally, they exhibit both negative and positive responses (Figure 8b, 8d).
414 Based on the results of factorial simulations and Mann-Kendall+Sen tests, CO₂ fertilization explains the
415 largest proportion of the change in the carbon stock; about 82.45% change in LVBC was positive (Figure
416 8a), whereas 89.28% of the change in WVBC was positive (Figure 8c). In factorial simulation S2, the
417 long-term trend of LVBC was $15.521 \text{ g C m}^{-2} \text{ yr}^{-1}$ and that of WVBC was $0.435 \text{ g C m}^{-2} \text{ yr}^{-1}$ at the
418 period from 1916 to 2015 (Figure A2a and Figure A3a). The separately simulated LVBC and WVBC
419 increased by 80.98 Pg C and 2.66 Pg C with increasing atmospheric CO₂ concentrations (from 301.73
420 ppm in 1916 to 400.83 ppm in 2015). The other climatic drivers (precipitation, temperature, radiation,
421 humidity, and wind speed) remained at baseline values. While the increase or decrease in the carbon
422 stock may be attributed to more than one driving factor, within any specified grid, the one with the highest

423 contribution was the driver that consistently resulted in the highest increase or decrease in the carbon
 424 stock for that grid. The spatial pattern illustrates that CO₂ dominates the variability in LVBC in 7.28%
 425 of the zones, including 1.21% of the zones that exhibited a negative change and 6.07% that exhibited a
 426 positive change (Figure 8b). CO₂ dominates the variability in WVBC in 27.60% of the zones, including
 427 1.73% of the zones that exhibited a negative change and 25.87% of zones with a positive change (Figure
 428 8d). Under the effect of CO₂ fertilization, grids with increased trend in WVBC mainly distribute in boreal
 429 latitudes (Figure 6c). These trends are consistent with and previous studies (Tharammal et al., 2019; Zhu
 430 et al., 2016; Keenan et al., 2017) in which positive trends occurred, especially for WVBC.

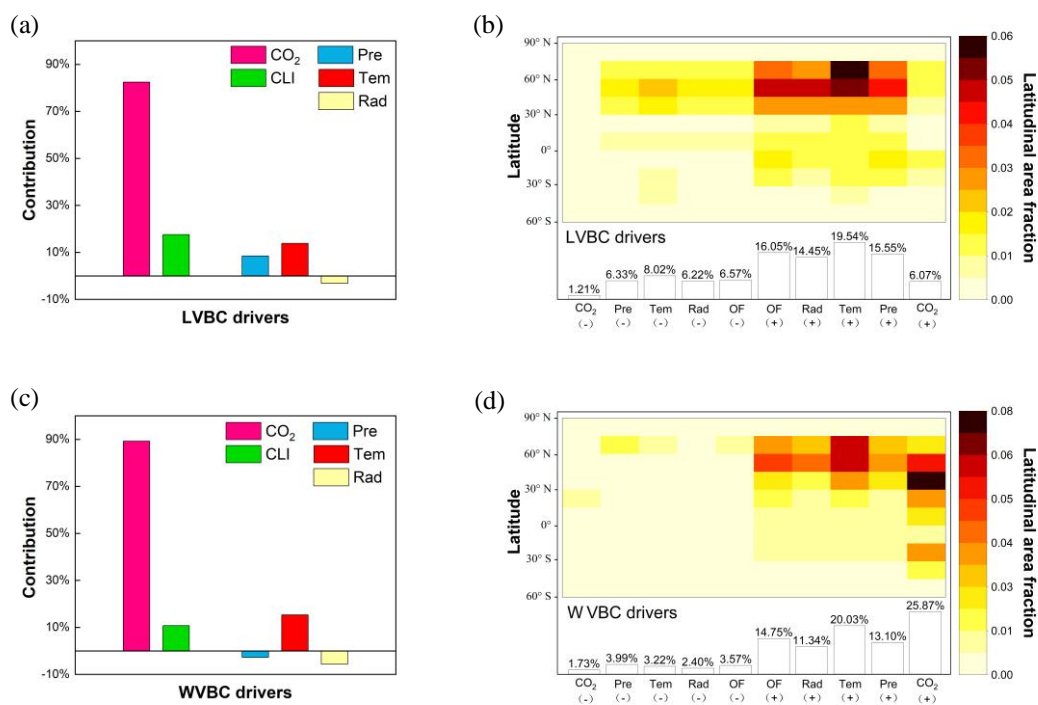


Figure 8. The proportion of change in the vegetation biomass carbon stocks attributed to driving factors. Ratios of the driving factors of CO₂ fertilization effects (CO₂), climate change effects (CLI), precipitation (Pre), temperature (Tem), radiation (Rad) for LVBC (a) and WVBC (c) under the five scenarios using the Mann-Kendall and Sen's slope estimator statistical tests. Attribution of LVBC (b) and WVBC (d) dynamics to driving factors calculated as averages along 15° latitude bands. At local scales, the driving factors include CO₂, Pre, Tem, Rad, and other climate factors (OF). A '+' symbol indicates a positive effect of the driving factor on carbon stock, and vice versa. The fraction of global area (%) that is predominantly influenced by the driving factors is shown at the top of the bar.

431 Climate change induced by the greenhouse effect explains part of the increase in carbon stocks, but unlike
432 CO₂ fertilization, climate has dramatic negative effects on some vegetated zones. Figure 8a illustrates
433 that temperature is the largest climatic contributor to the change in LVBC (13.83%, 2.572 g m⁻² yr⁻¹),
434 followed by precipitation (8.51%, 1.572 g m⁻² yr⁻¹) and radiation (-3.19%, -0.649 g m⁻² yr⁻¹). The spatial
435 distribution shows that temperature predominantly influences the change in LVBC (Figure 8b),
436 influencing over 27.56% of the global vegetated zones, followed by precipitation (21.88%) and radiation
437 (20.67%). Figure 8c shows there is a difference in the negative contribution of precipitation to the change
438 in WVBC at the global level (-2.76%, -0.013 g m⁻² yr⁻¹). Temperature is the largest climatic contributor
439 to the change in WVBC (15.36%, 0.075 g m⁻² yr⁻¹), followed by radiation (-5.63%, -0.027 g m⁻² yr⁻¹).
440 Modelled WVBC trends based on the factorial simulations have similar spatiotemporal patterns to LVBC
441 (Figures A2 and A3), the spatial patterns of light- and water-gathering carbon stocks show a significant
442 increasing trend in the most of boreal zones. In the Southern Hemisphere, the trends of WVBC are
443 extensively statistically insignificant in all factorial simulations, and only a small proportion of grids
444 show a significantly increasing trend. There is a significantly increasing trend in LVBC in south-central
445 Africa and northern South America. The effects of temperature on WVBC are stronger than LVBC,
446 because temperature has a stronger effect on the metabolism process of root growth, dominating the
447 turnover rate and the costs of maintenance respiration in root growth process (Gill and Jackson, 2000).
448 It should be noted that trends in the global carbon stock can be largely attributed to the influences of CO₂,
449 precipitation, temperature, and radiation (Figure 8). Nonetheless, at the zonal scale, the contributions of
450 other factors should be considered, such as humidity and wind speed. The effects of these other factors
451 dominate trends in LVBC in over 16.05% of the zones that increased and 6.57% of the zones that
452 decreased. In the case of changes in WVBC, other factors were dominant drivers in over 14.75% of the
453 zones that increased and 3.57% of zones that decreased. Under the effect of climate, the variability of
454 LVBC and WVBC is positive in most zones, promoting the noticeable increase of carbon stocks in boreal
455 latitudes.

456 **3.5 Constraints imposed by water limitations**

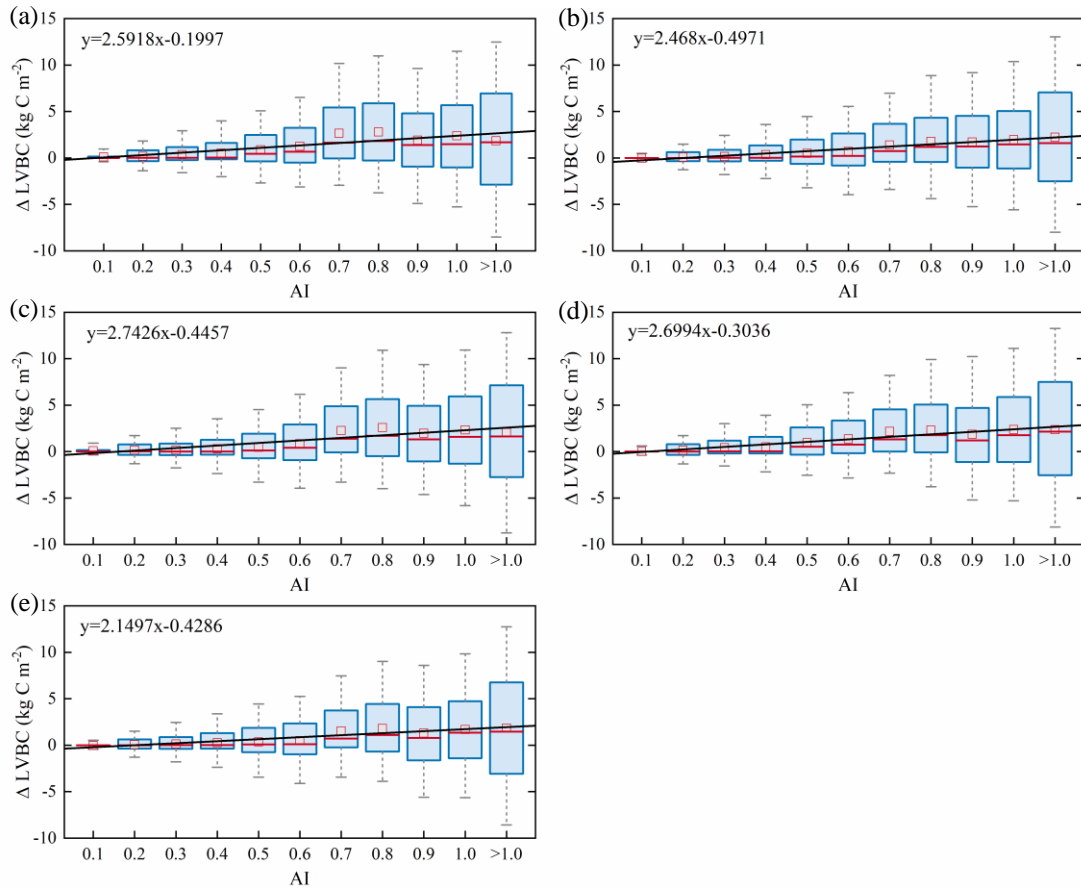


Figure 9. Relationships in the incremental change between AI and LVBC over the hydrological zones. Magnitude of change in LVBC in the historical scenario S1 (a), CO₂ in scenario S2 (b), CO₂ + precipitation in scenario S3 (c), CO₂ + temperature in scenario S4 (d), and CO₂ + radiation in scenario S5 (e). Range of the box is 25%-75% of values; range of the whiskers is 10%-90% of values; the small red square is average value; the red line is the median line; and the black line is the fitted curve. Positive value of the Y axis represents the magnitude of increased LVBC from 1916 to 2015 under water-limitations conditions, and vice verse.

457 Terrestrial water availability emerged as a key regulator of terrestrial carbon storage, by affecting the
 458 response mechanism of the vegetation carbon stock to changes in driving factors. As shown in Figures 9
 459 and 10, with an increase in the aridity index (i.e., an increase in available water), the magnitude and range
 460 in variations of LVBC density and WVBC density gradually enhance. Based on the results of factorial
 461 simulations, we find a positive relationship between LVBC and water pressure. In extreme water stress,
 462 the increase of LVBC tends to zero and plants stop growing. There is no obvious different in the slopes

463 of fitting curves between factorial simulations. The pattern of the enhanced magnitude and range of
464 variation in the WVBC density is unimodal with water stress gradient in all factorial simulations. With
465 the increasing of AI, the magnitude of change in WVBC increases at first and then decreases finally. The
466 mitigation of water stress promotes WVBC increase, while excess surface water limits the response of
467 WVBC to changes in climate and CO₂. These results reveal that the carbon stock increases stimulated by
468 changes in climate and CO₂ are constrained by water available. With increased warming, water
469 limitations are expected to increasingly limit the carbon stock increase, specially at arid regions. To
470 further reveal the controls of water limitation on the responses of inner carbon storages to each driver,
471 we analyse the long-term variability of potential vegetation carbon stocks by means of factorial
472 simulations for each hydrological region (Figure 1). It is revealed from Figure A6 that the increased
473 LVBC density induced by drivers changed from $0.878 \pm 0.131 \text{ kg C m}^{-2}$ in the hyper-arid regions to
474 $5.459 \pm 0.610 \text{ kg C m}^{-2}$ in the humid regions during the past hundred years. At global scale, the annual
475 mean value of LVBC simulated by each factorial simulation is close. In hyper-arid and arid regions, the
476 interannual change of LVBC in historical scenario matchs most closely with that of S3 scenario which
477 considers CO₂ and precipitation effects. Increased WVBC density induced by drivers changed from 0.011
478 $\pm 0.001 \text{ kg C m}^{-2}$ in the hyper-arid regions to $0.044 \pm 0.005 \text{ kg C m}^{-2}$ in the humid regions during the
479 same period (Figure A7). The long-term trends of WVBC simulated by each scenario are consistent
480 across different hydrological regions. With a lessening of water stress (from hyper-arid to humid region),
481 the response of the carbon stock to changes in climate and CO₂ gradually became more noticeable. The
482 robust pattern in the zonal average density of the carbon stock shows that terrestrial water limitations
483 strongly limit the enhanced magnitude of the carbon stock.

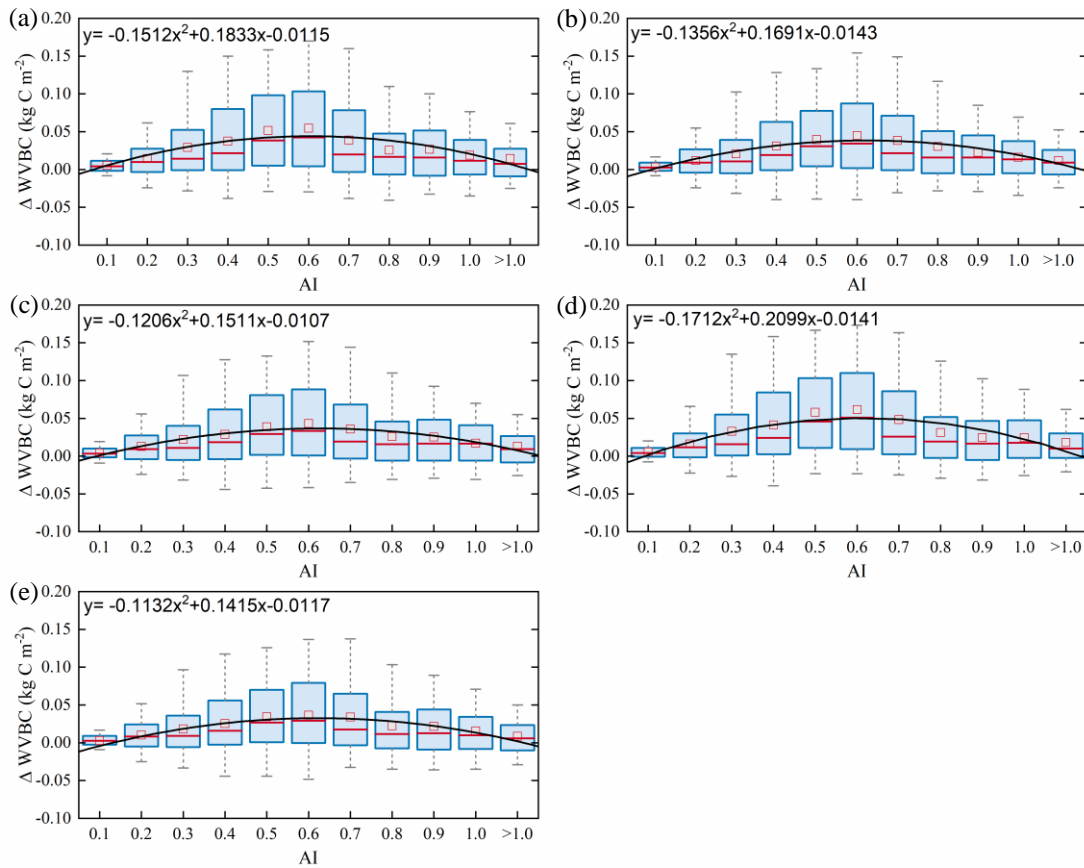


Figure 10. Relationships in the incremental change in AI and WVBC over the hydrological regions. Modelled WVBC enhanced magnitude in the historical scenario S1 (a), CO₂ in scenario S2 (b), CO₂ + precipitation in scenario S3 (c), CO₂ + temperature in scenario S4 (d), and CO₂ + radiation in scenario S5 (e). Range of the box is 25%-75% of values; range of the whiskers is 10%-90% of values; the small red square is average value; the red line is the median line, and the black line is the fitted curve. Positive value of the Y axis represents the magnitude of increased WVBC from 1916 to 2015 under water-limitations conditions, and vice versa.

484 Water limitations not only directly reduced the magnitude of the response in the two fractions' carbon
 485 stock (LVBC and WVBC) to changes in climate and CO₂, but also indirectly confined the response
 486 direction of each fractions' carbon stock by transforming vegetation structure and function. Figure 11
 487 illustrates temporal variations in the carbon stock ratio within and between hydrological regions. From
 488 hyper-arid region to humid region, the variation range of ratio between LVBC and WVBC significantly
 489 increases. Plants store more assimilated carbon in shoots and leaves in humid regions. The long-term
 490 effects of driver changes have a positive influence on this carbon allocate pattern. Under the synergistic
 491 effect of drivers and water stress, vegetation carbon stock increases, and there is a larger proportion of

492 biomass allocated to, and stored in, light-gathering vegetation organs. In drylands ($AI \leq 0.5$) of all
 493 factorial simulations, light- and water-gathering biomass carbon stocks both increased but the rate of
 494 change in the LVBC/WVBC ratio gradually decreased. To mitigate water stress, plants allocate more
 495 assimilated carbon to root for gathering water. In humid zones ($AI > 0.65$), the proportion of LVBC
 496 increases more than that of WVBC to obtain more resources like CO_2 and radiation energy, leading to
 497 an increase in the LVBC/WVBC ratio.

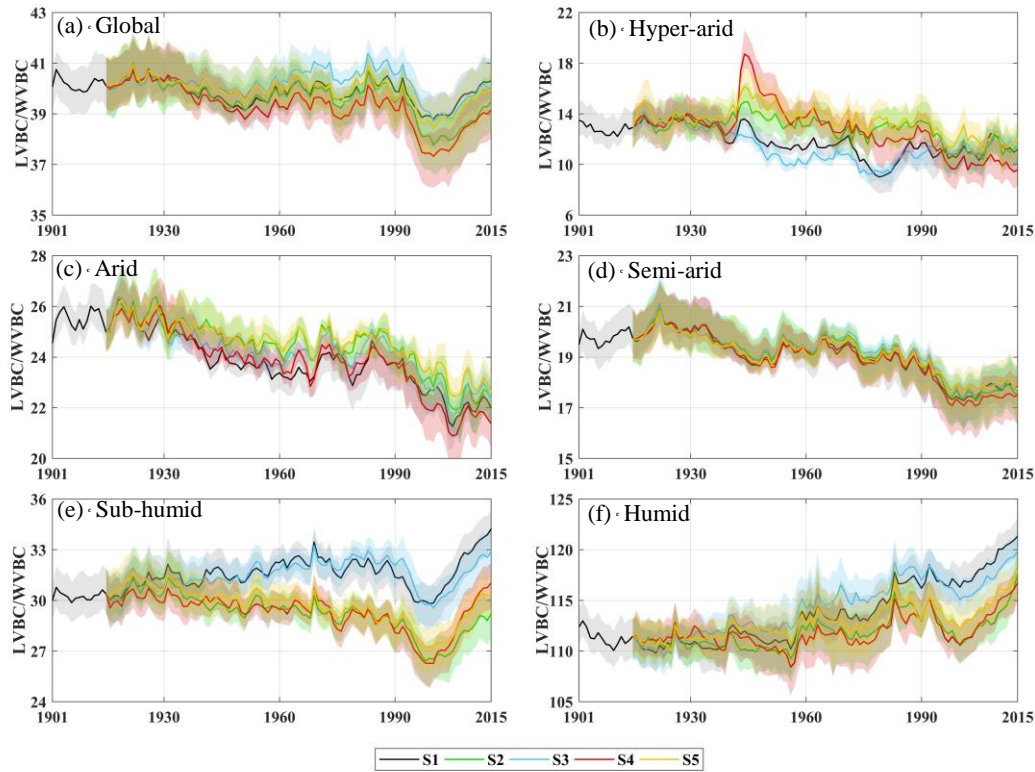


Figure 11. Temporal fluctuations in carbon stock dynamics in vegetation biomass in different factorial simulations. Black indicates historical factorial simulation from 1901-2015, green indicates the CO_2 -driven factorial simulation, blue indicates the precipitation-driven factorial simulation, red indicates the temperature-driving factorial simulation and yellow indicates radiation driven factorial simulation. Uncertainty bounds are provided as shaded areas reflect the intra-annual fluctuation (± 1 s.d.) (a) Modelled trend of LVBC/WVBC ratio in Global area. (b-f) Modelled trend of the LVBC/WVBC ratio in different hydrological regions.

498 **4 Discussions and conclusion**

499 To understand the response of carbon storage potential and its inner biomass carbon stocks to

500 environmental change, we conducted a series of factorial simulations using SEIB-DGVM V3.02. More
501 importantly, we investigated the extent of the responses of carbon stocks to water limitations.

502

503 Over the past 100 years, there has been an ongoing increase in the carbon storage capacity of the
504 terrestrial ecosystem from 735 Pg C in 1916 to 855 Pg C in 2015, which has slowed the rate at which
505 atmospheric CO₂ has increased and may have mitigated global warming. These findings are consistent
506 with the conclusions of research conducted at the local scale. For example, based on carbon flux data,
507 Erb et al. (2008) suggested that the vegetation carbon stock in Austria increased from 1043 Mt C to 1249
508 Mt C (aboveground carbon stocks growth was 1.059 Mt C yr⁻¹ and belowground carbon stocks growth
509 was 0.2 Mt C yr⁻¹) since industrialization. Le Noë et al. (2020) showed that increases in the carbon stocks
510 and carbon density were the predominant drivers in the forest terrestrial carbon sequestration capacity in
511 France from 1850 to 2015. Tong et al. (2020) also found a substantial increase of aboveground carbon
512 stocks in southern China (0.11 Pg C yr⁻¹) during the period 2002–2017. However, these studies focused
513 on zonal trends in total vegetation carbon stocks and did not investigate the extent of the response in
514 vegetation carbon stocks partitioned between light- and water-gathering biomass. Our results show that
515 the increase in carbon stock in light-gathering vegetation organs was much larger than that in water-
516 gathering vegetation organs, and light-gathering biomass carbon stock dominates the historical trend of
517 the terrestrial carbon stock. During the past decades, the global land surface has been greening because
518 of the flux and storage of more carbon into plant trunks and foliage (Zhu et al., 2016). Compared with
519 WVBC, LVBC increase 116.18 ± 2.34 Pg C and dominates the long-term trends of vegetation carbon
520 stock. The latitudinal bands of increasing annual LVBC are mainly distributed in tropical latitudes, a
521 conclusion consistent with prior knowledge that tropical zones dominate carbon uptake and storage (Erb
522 et al., 2018; Schimel et al., 2015). Biomass carbon allocation between light- and water-gathering
523 vegetation organs reflect the changes in individual growth, community structure and ecosystem function,
524 which are important attributes in the investigation of carbon stocks and carbon cycling within the
525 terrestrial biosphere (Hovenden et al., 2014; Fang et al., 2010; Ma et al., 2021). During the past hundred
526 years, the ratio of LVBC/WVBC shown a slight upward trend. The rate of increase is 0.0171 yr⁻¹, which
527 is significant at the 0.01 level. To better absorb CO₂ and sunlight required for photosynthesis, vegetated
528 regions are gradually covered by vegetation with higher plant height and wider leaf area, thereby

529 adjusting their characteristic ecosystem functions (Anderson et al., 2010).

530

531 Based on our factorial simulations, the vegetation carbon stock exhibited the most increase under the
532 influence of CO₂ fertilization. In addition, the responses of carbon stocks to climatic factors of change
533 differed, particularly at the zonal scale (Figure 8). Previous studies have pointed out that the variation of
534 the terrestrial carbon stock caused by releasing or sequestering carbon is sensitive to anomalous changes
535 in water availability and light use efficiency (Madani et al., 2020; Humphrey et al., 2018). At local scale,
536 radiation dominated the long-term trend of LVBC in 20.67% of global zones and that of WVBC in
537 13.74%, while precipitation dominated the long-term trend of LVBC in 21.88% of global zones and that
538 of WVBC in 17.09% of global zones. However, radiation induced light variation in LVBC (-3.19%) and
539 WVBC (-5.62%) at global scale. Precipitation explain 8.51% of LVBC trend and -2.76% of WVBC trend
540 at global scale. LVBC and WVBC variations driven by precipitation and radiation were ultimately offset
541 by spatially compensatory effects, which dampened the response of the carbon stock to these factors at
542 global scale (Jung et al. 2017). Trend in temperature drove historical long-term trends in the potential
543 carbon stocks, with faster increases and considerable variation occurring by zone. The accumulated
544 influence of climate warming induces dramatic changes in the carbon stock at a global scale. Thus, our
545 results revealed that temperature dominates the long-term trends in the carbon stock among climatic
546 drivers, while a compensatory effect exists in the global change in the carbon stock induced by
547 precipitation and radiation.

548

549 By partitioning the trends of LVBC and WVBC into five hydrological regions (Figure 1), we found that
550 the long-term change in carbon stocks is tightly coupled to terrestrial water availability. These results
551 indicate that vegetation in humid region is responsible for most of the trend in global LVBC, while plants
552 in semi-arid region play a dominate global role in controlling the long-term trend in WVBC. As water
553 stress decreases, the magnitude and range in variation of LVBC gradually increase (Figure 9), which
554 suggests that limited water availability constrains the response magnitude of the changes in LVBC to
555 changes in CO₂ and climate. The response pattern of WVBC growth to the increasing water availability
556 is different from that of LVBC. Drought mitigation promotes the growth of WVBC, while humid region
557 with high light competition limits root growth. The result is consistent with previous finding that plants

558 reduce allocation to roots in dense forests where aboveground competition for light is high (Ma et al.
559 2021). Moreover, we found that indirect effects of water limitation regulate increasing rate of each carbon
560 pool. Although vegetation carbon stocks dramatically increase under the effects of climate and CO₂
561 changes, the increasing rate of LVBC faster than WVBC in humid region. Vegetation stores more
562 biomass in aboveground plant organs (trunk and foliage) to gather light. Dryland vegetation decrease the
563 LVBC/WVBC ratios and stores more biomass below ground to enhance the capture of water resources.
564 Based on these results, we demonstrated that water limitations controlled the variable response of
565 terrestrial vegetation carbon stocks. Our findings are consistent with other reports about the impact of
566 increasing water limitations on terrestrial ecosystem. Based on satellite remote sensing observations,
567 Madani et al. (2020) found that changes in water constraints can lead to variable responses in ecosystem
568 productivity and net carbon exchange. Humphrey et al. (2021) found that increasing water stress limits
569 the response magnitude of carbon uptake rates through a down-regulation of stomatal conductance and
570 suggested that land carbon uptake is driven by temperature and vapour pressure deficit effects that are
571 controlled by terrestrial water availability. Ma et al. (2021) found that plants increase investment into
572 building roots in arid region because the extent of water limitation there is exacerbated by global warming.
573 Terrestrial ecosystems utilize sensitive strategies to allocate and store biomass to adjust to local
574 hydrological conditions. A significant conclusion is that water constraints not only confine the responses
575 of vegetation carbon stocks to drivers of variability, but also constrain the proportion of biomass carbon
576 stocks in gather- and water-gathering fractions.

577

578 Distinguishing the response of carbon stock fractions estimated by SEIB-DGVM improves the
579 understanding of the interactive impacts of terrestrial carbon and water dynamics. However, uncertainty
580 still exists because of the limitations in the processes of modelling vegetation metabolism with SEIB-
581 DGVM. Trunk biomass contains tree branches and structural roots (coarse roots and tap roots) (Sato et
582 al., 2007), so the R/S ratio of potential vegetation in factorial simulations is smaller than the R/S of actual
583 vegetation in observation stations. Root biomass only contains the fine root biomass, leading to an
584 underestimate in belowground organ biomass of trees and grasses compare with previous conclusion (Ma
585 et al., 2021; Yang et al., 2009). Availability of nitrogen is a key limiting factor for vegetation growth,
586 especially when higher CO₂ fertilization effects exist (Tharammal et al., 2019). The limitation could be

587 alleviated by nitrogen deposition in most temperate and boreal ecosystems. The SEIB-DGVM
588 experiments were conducted with a focus on documenting CO₂ fertilization and climate change
589 interactions; these experiments did not consider the influences of nitrogen deposition, which leads to a
590 slight overestimate of the contributions of CO₂ fertilization on biomass production.

591

592 In summary, we evaluated SEIB-DGVM V3.02 and used this model to offer new perspectives on the
593 response of vegetation carbon storage potential to changes in climate and CO₂. Our simulation results
594 show that changes in CO₂, rather than climate, dominate the light- to water-gathering partitioning of the
595 carbon storage potential. More importantly, we suggest that the impact of CO₂ fertilization and
596 temperature effects on vegetation carbon-sequestration potential depends on water availability and its
597 impacts on plant stress. With increased global warming, water limitations are expected to increasingly
598 confine global carbon sequestration and storage. Our findings highlight the need to account for terrestrial
599 water limitation effects when estimating the response of the terrestrial carbon storage capacity to global
600 climate change, and the need for stronger interactions between those involved in vegetation model
601 development and those in between the hydrological and ecological research communities.

603 **Table A1. MCD12C1 legend and class descriptions**

Name	Value	Description
Evergreen Needleleaf Forests	1	Dominated by evergreen conifer trees (canopy >2m). Tree cover >60%.
Evergreen Broadleaf Forests	2	Dominated by evergreen broadleaf and palmate trees (canopy >2m). Tree cover >60%.
Deciduous Needleleaf Forests	3	Dominated by deciduous needleleaf (larch) trees (canopy >2m). Tree cover >60%.
Deciduous Broadleaf Forests	4	Dominated by deciduous broadleaf trees (canopy >2m). Tree cover >60%.
Mixed Forests	5	Dominated by neither deciduous nor evergreen (40-60% of each) tree type (canopy >2m). Tree cover >60%.
Closed Shrublands	6	Dominated by woody perennials (1-2m height) >60% cover.
Open Shrublands	7	Dominated by woody perennials (1-2m height) 10-60% cover.
Woody Savannas	8	Tree cover 30-60% (canopy >2m).
Savannas	9	Tree cover 10-30% (canopy >2m).
Grasslands	10	Dominated by herbaceous annuals (<2m).
Permanent Wetlands	11	Permanently inundated lands with 30-60% water cover and >10% vegetated cover.
Croplands	12	At least 60% of area is cultivated cropland.
Urban and Built-up Lands	13	At least 30% impervious surface area including building materials, asphalt, and vehicles.
Cropland/Natural Vegetation Mosaics	14	Mosaics of small-scale cultivation 40-60% with natural tree, shrub, or herbaceous vegetation.
Permanent Snow and Ice	15	At least 60% of area is covered by snow and ice for at least 10 months of the year.
Barren	16	At least 60% of area is non-vegetated barren (sand, rock, soil) areas with less than 10% vegetation.
Water Bodies	17	At least 60% of area is covered by permanent water bodies.
Unclassified	255	Has not received a map label because of missing inputs

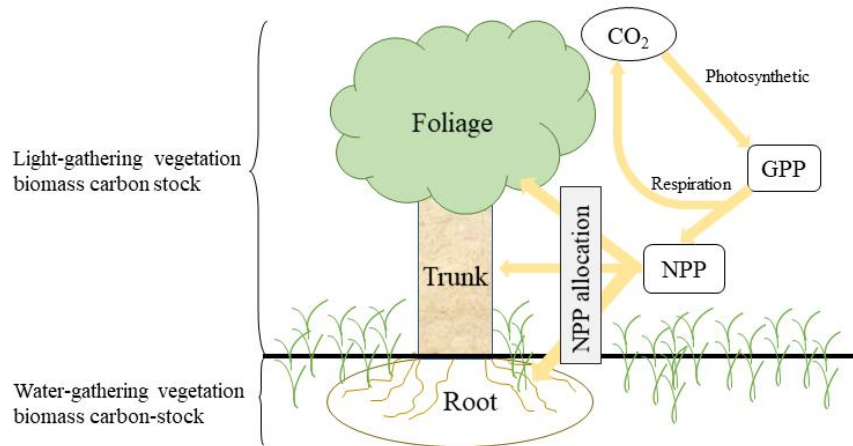


Figure A1. Schematic of ecosystem carbon cycle. Yellow arrow indicates carbon flux. Atmospheric CO₂ transitions into gross primary production (GPP) by photosynthesis. GPP is partitioned into respiration and net primary production (NPP). NPP is partitioned into three biomass carbon pools (foliage, trunk, and root).

605

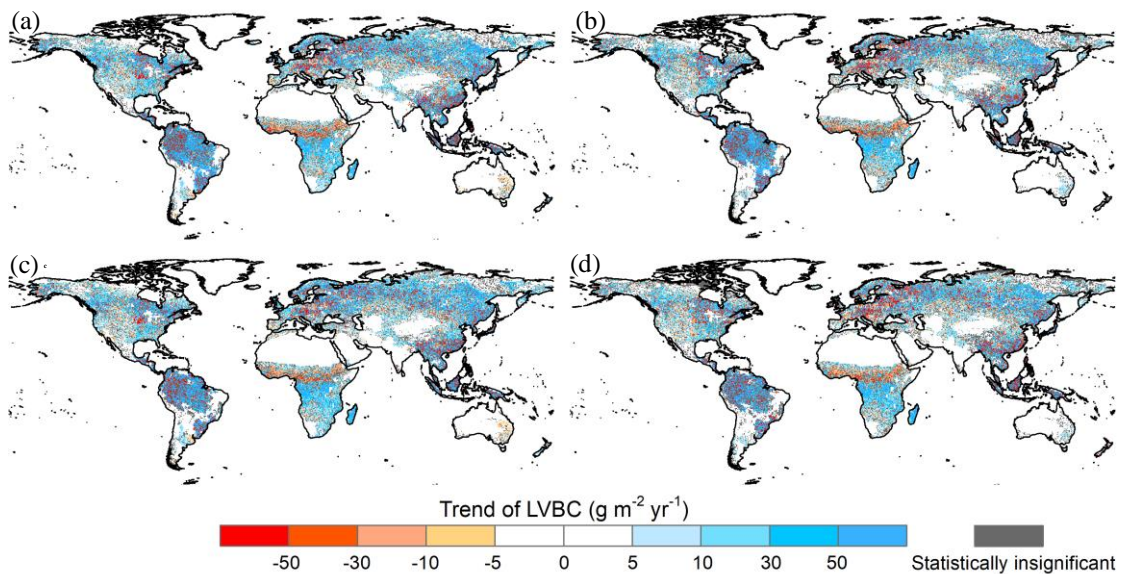


Figure A2. Potential LVBC trend maps during the period of 1916 to 2015 under different factorial simulations. (a) CO₂ driving factorial simulation; (b) CO₂+precipitation driving factorial simulation. (c) CO₂+temperature driving factorial simulation; and (d) CO₂+radiation driving factorial simulation. Positive values indicate increasing trends in the ratio, and vice versa. All results from Mann-Kendall and Sen's slope statistical tests correspond to the 95% confidence interval.

606

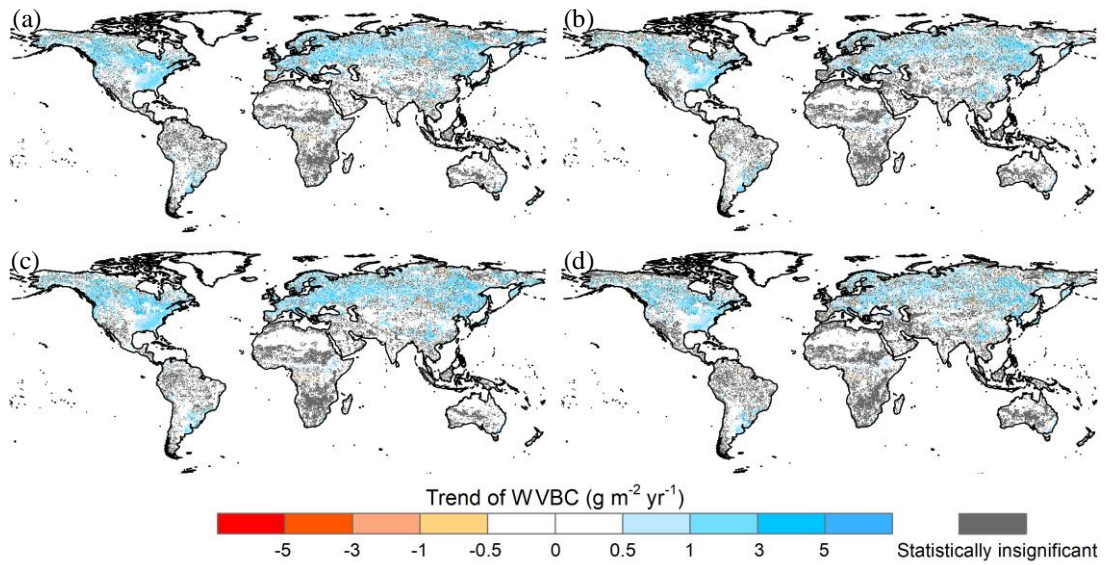


Figure A3. Potential WVBC variation trend maps during the period of 1916 to 2015 under different factorial simulations. (a) CO₂ driving factorial simulation; (b) CO₂+precipitation driving factorial simulation. (c) CO₂+temperature driving factorial simulation; and (d) CO₂+radiation driving factorial simulation. Positive values indicate increasing trends in the ratio, and vice versa. All results from Mann-Kendall and Sen's slope statistical tests correspond to the 95% confidence interval.

607

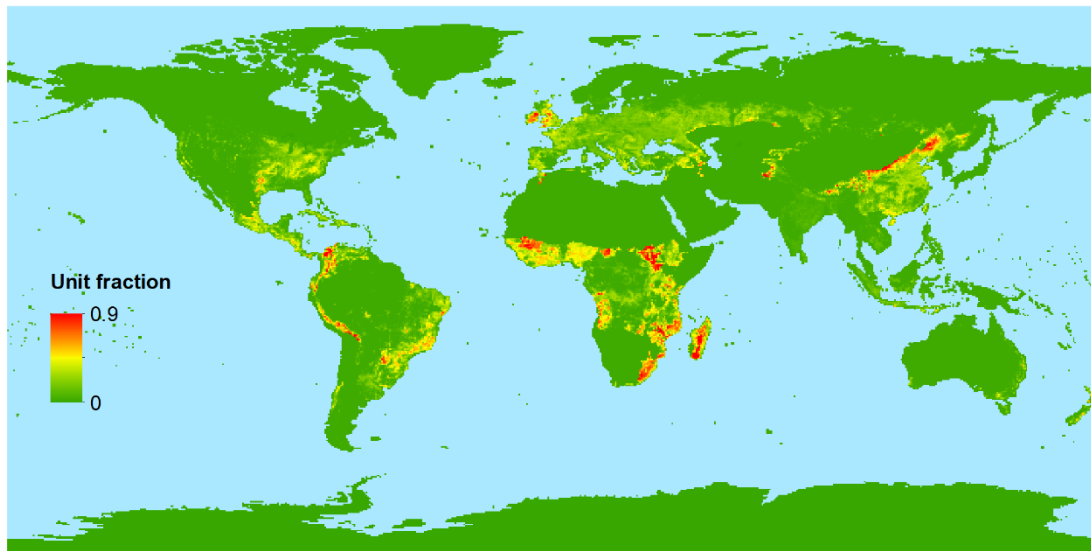


Figure A4. Spatial distribution of multi-year average fraction of managed pasture from 2001-2015 at 0.5×0.5 arc-degree resolution.

608

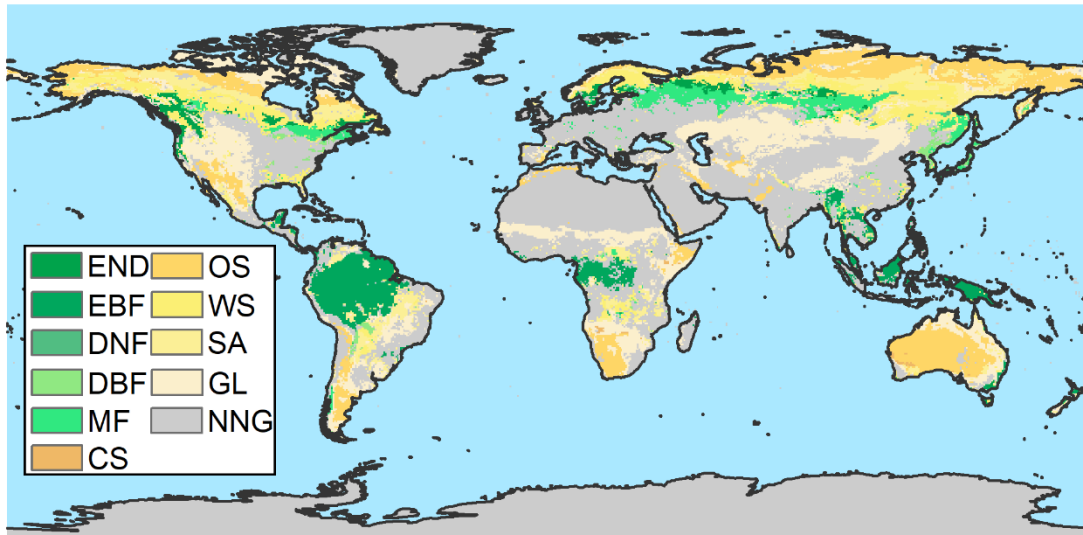


Figure A5. Map of land vegetation without anthropogenic disturbance from MCD12C1 and LUH2. END: Evergreen needleleaf forest, EBF: Evergreen broadleaf forest, DNF: Deciduous needleleaf forest, DBF: Deciduous broadleaf forest, MF: Mixed forest, CS: Closed shrublands, OS: Open shrublands, WS: Woody savannas, SA: Savannas, GL: Grasslands, NNG: No natural vegetation, which means the zone is not covered by vegetation without anthropogenic disturbance.

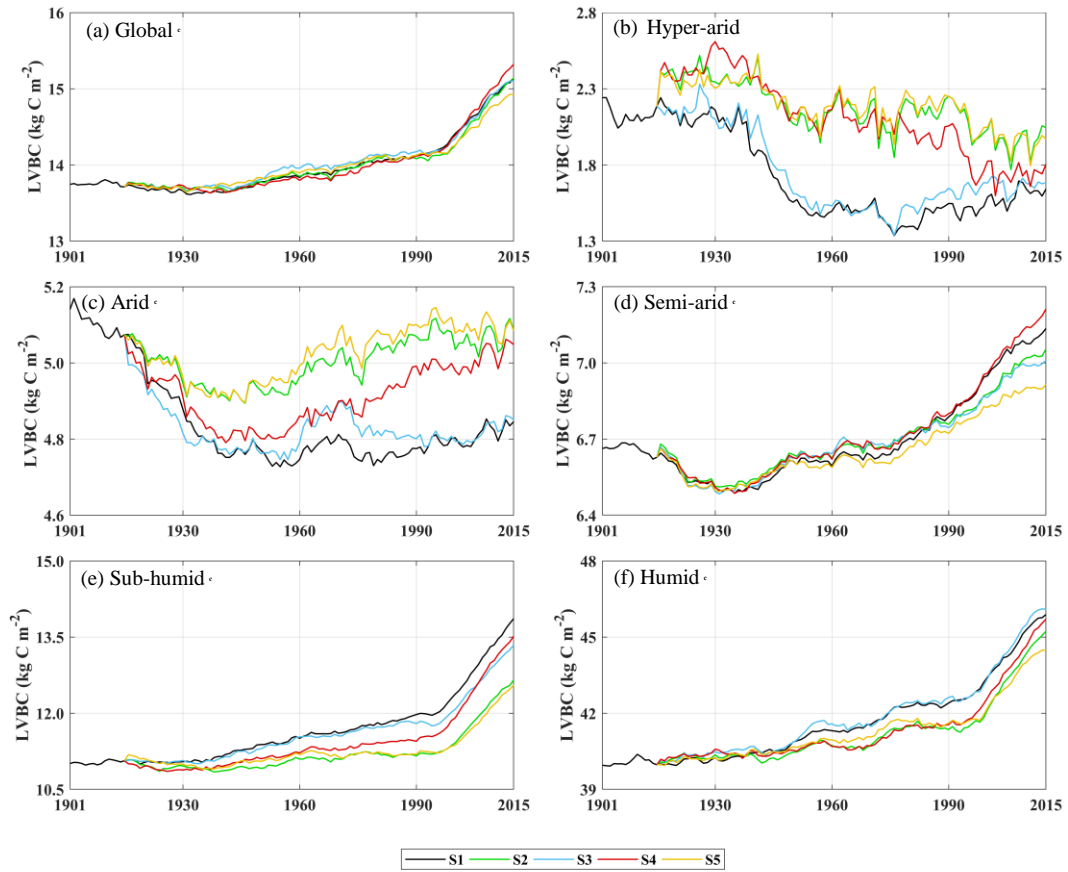


Figure A6. Trends in average density of potential LVBC. (a) Modelled trend of annual averaged LVBC globally. Modelled trends in annual averaged LVBC in hyper-arid zone (b), arid zone (c), semi-arid zone (d), sub-humid zone (e), and humid zone (f).

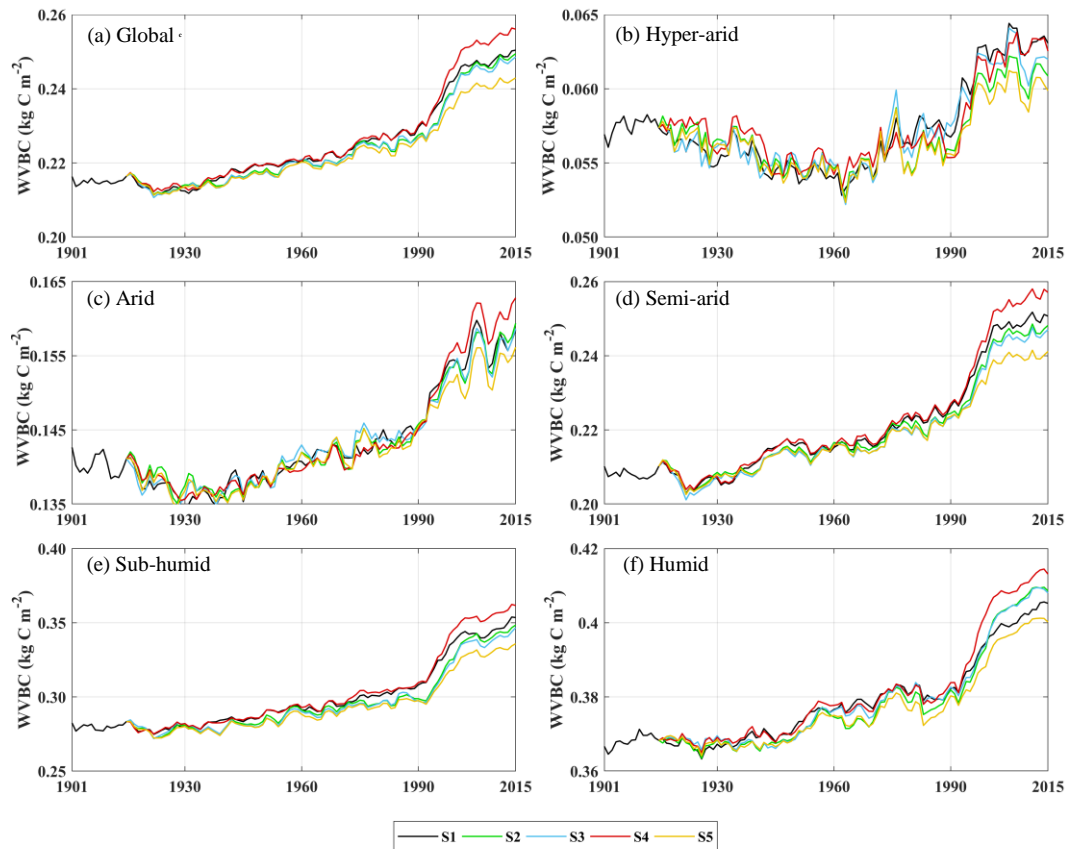


Figure A7. Trends in average density of potential WVBC. (a) Modelled trend of annual averaged WVBC globally. Modelled trends in annual averaged WVBC in hyper-arid zone (b), arid zone (c), semi-arid zone (d), sub-humid zone (e), and humid zone (f).

611 **Code and data availability statement**

612 The code of SEIB-DGVM version 3.02 can be download from <http://seib-dgvm.com/>. Climatic Research
 613 Unit data can be downloaded from <https://crudata.uea.ac.uk/cru/data/hrg/>. The soil physical parameters
 614 can be downloaded from www.iges.org/gswp. The reconstructed CO₂ concentration dataset and SEIB
 615 code can be downloaded from <http://seib-dgvm.com/>. In model validation, Ecosystem Model-Data
 616 Intercomparison (multiyear average NPP product) data were collected from
 617 https://daac.ornl.gov/NPP/guides/NPP_EMDI.html. Remote sensing product MOD17A3 data were
 618 obtained from <https://lpdaac.usgs.gov/products/mod17a3hgf006/>, MCD12C1 data were obtained from
 619 <https://ladsweb.modaps.eosdis.nasa.gov/search/order>, and LUH2 data were obtained from
 620 <https://luh.umd.edu/>.

621 **Authors contributions**

622 T.S. designed research. T.S., and S.H. performed research and developed the methodology. T.S. analyzed
623 data and produced the outputs. T.S., S.H., C.J., and X.C. wrote the first manuscript draft. W.W. and W.G.
624 supervised the study. All the authors discussed the methodology and commented on various versions of
625 the manuscript.

626 **Competing interests**

627 The authors declare that they have no conflict of interest.

628 **Acknowledgments**

629 This work was jointly supported by the National Natural Science Foundation of China (Grant Nos.
630 51979071, 51779073, 91547205), the National Key Research and Development Program of China
631 (2021YFC3201100), the Distinguished Young Fund Project of Natural Science Foundation of Jiangsu
632 Province (BK20180021), and the National “Ten Thousand Program” Youth Talent. We thank Zefeng
633 Chen for technical support. We gratefully thank the following data providers and model developers for
634 their continuous efforts and for sharing their data: the University of East Anglia, the National Centers for
635 Environmental Prediction (NCEP), the National Oceanic and Atmospheric Administration (NOAA),
636 University of Maryland, and the Center for Ocean-Land-Atmosphere Studies (COLA). Cordial thanks
637 are extended to the editor, Dr. Hans Verbeeck, and two anonymous referees for the valuable comments
638 which greatly improve the quality of the paper.

639 **References**

- 640 Ahlstrom, A., Raupach, M. R., Schurgers, G., Smith, B., Arneeth, A., Jung, M., Reichstein, M., Canadell,
641 J. G., Friedlingstein, P., Jain, A. K., Kato, E., Poulter, B., Sitch, S., Stocker, B. D., Viovy, N., Wang,
642 Y. P., Wiltshire, A., Zaehle, S., and Zeng, N.: The dominant role of semi-arid ecosystems in the
643 trend and variability of the land CO₂ sink, *Science*, 348, 895-899, 10.1126/science.aaa1668, 2015.
- 644 Ajtay, G. L., Ketner, P., and Duvigneaud, P.: Terrestrial primary production and phytomass In: *The*
645 *Global Cycle.*, Glob. Carbon Cycle, SCOPE, 129-181 pp.1979.
- 646 Anderson, L. J., Derner, J. D., Polley, H. W., Gordon, W. S., Eissenstat, D. M., and Jackson, R. B.: Root
647 responses along a subambient to elevated CO₂ gradient in a C₃-C₄ grassland, *Global Change Biol*,
648 16, 454-468, 10.1111/j.1365-2486.2009.01975.x, 2010.
- 649 Bartholome, E. and Belward, A. S.: GLC2000: a new approach to global land cover mapping from Earth
650 observation data, *Int J Remote Sens*, 26, 1959-1977, 10.1080/01431160412331291297, 2005.
- 651 Bayer, A. D., Pugh, T. A. M., Krause, A., and Arneeth, A.: Historical and future quantification of
652 terrestrial carbon sequestration from a Greenhouse-Gas-Value perspective, *Global Environmental*
653 *Change*, 32, 153-164, 10.1016/j.gloenvcha.2015.03.004, 2015.
- 654 Bazilevich, N. I., Rodin, L. Y., and Rozov, N. N.: Geographical Aspects of Biological Productivity,
655 *Soviet Geograpy Review and Translation*, 5, 293-317 pp.1971.
- 656 Bloom, A. A., Exbrayat, J. F., van der Velde, I. R., Feng, L., and Williams, M.: The decadal state of the
657 terrestrial carbon cycle: Global retrievals of terrestrial carbon allocation, pools, and residence times,
658 *Proceedings of the National Academy of Sciences of the United States of America*, 113, 1285-1290,
659 10.1073/pnas.1515160113, 2016.
- 660 Chen, J., Ju, W., Ciais, P., Viovy, N., Liu, R. G., Liu, Y., and Lu, X. H.: Vegetation structural change
661 since 1981 significantly enhanced the terrestrial carbon sink, *Nat Commun*, 10, 4259,
662 10.1038/S41467-019-12257-8, 2019.
- 663 Chen, L.-P., Zhao, N.-X., Zhang, L.-H., and Gao, Y.-B.: Responses of two dominant plant species to
664 drought stress and defoliation in the Inner Mongolia Steppe of China, *Plant Ecology*, 214, 221-229,
665 10.1007/s11258-012-0161-y, 2013.
- 666 Cheng, L., Zhang, L., Wang, Y. P., Canadell, J. G., Chiew, F. H. S., Beringer, J., Li, L. H., Miralles, D.
667 G., Piao, S. L., and Zhang, Y. Q.: Recent increases in terrestrial carbon uptake at little cost to the
668 water cycle, *Nat Commun*, 8, 10.1038/s41467-017-00114-5, 2017.
- 669 Erb, K.-H., Gingrich, S., Krausmann, F., and Haberl, H.: Industrialization, Fossil Fuels, and the
670 Transformation of Land Use, *Journal of Industrial Ecology*, 12, 686-703, 10.1111/j.1530-
671 9290.2008.00076.x, 2008.
- 672 Erb, K.-H., Gaube, V., Krausmann, F., Plutzer, C., Bondeau, A., and Haberl, H.: A comprehensive global
673 5min resolution land-use data set for the year 2000 consistent with national census data, *Journal of*
674 *Land Use Science*, 2, 191-224, 10.1080/17474230701622981, 2007.
- 675 Erb, K.-H., Fetzel, T., Plutzer, C., Kastner, T., Lauk, C., Mayer, A., Niedertscheider, M., Körner, C., and
676 Haberl, H.: Biomass turnover time in terrestrial ecosystems halved by land use, *Nat Geosci*, 9, 674-
677 678, 10.1038/ngeo2782, 2016.
- 678 Erb, K.-H., Kastner, T., Plutzer, C., Bais, A. L. S., Carvalhais, N., Fetzel, T., Gingrich, S., Haberl, H.,
679 Lauk, C., Niedertscheider, M., Pongratz, J., Thurner, M., and Luyssaert, S.: Unexpectedly large
680 impact of forest management and grazing on global vegetation biomass, *Nature*, 553, 73-76,
681 10.1038/nature25138, 2018.

682 Fan, L., Wigneron, J. P., Ciais, P., Chave, J., Brandt, M., Fensholt, R., Saatchi, S. S., Bastos, A., Al-
683 Yaari, A., Hufkens, K., Qin, Y. W., Xiao, X. M., Chen, C., Myneni, R. B., Fernandez-Moran, R.,
684 Mialon, A., Rodriguez-Fernandez, N. J., Kerr, Y., Tian, F., and Penuelas, J.: Satellite-observed
685 pantropical carbon dynamics, *Nat Plants*, 5, 944-951, 10.1038/s41477-019-0478-9, 2019.

686 Fang, J., Yang, Y., Ma, W., Mohammat, A., and Shen, H.: Ecosystem carbon stocks and their changes
687 in China's grasslands, *Science China. Life sciences*, 53, 757-765, 10.1007/s11427-010-4029-x, 2010.

688 Friedlingstein, P., Joel, G., Field, C. B., and Fung, I. Y.: Toward an allocation scheme for global
689 terrestrial carbon models, *Global Change Biol*, 5, 755-770, DOI 10.1046/j.1365-2486.1999.00269.x,
690 1999.

691 Gentine, P., Green, J. K., Guérin, M., Humphrey, V., Seneviratne, S. I., Zhang, Y., and Zhou, S.:
692 Coupling between the terrestrial carbon and water cycles—a review, *Environ Res Lett*, 14, 083003,
693 10.1088/1748-9326/ab22d6, 2019.

694 Gill, R. and Jackson, R.: Global patterns of root turnover for terrestrial ecosystems, *New Phytol*, 147,
695 13-31, 10.1046/j.1469-8137.2000.00681.x, 2000.

696 Gocic, M. and Trajkovic, S.: Analysis of changes in meteorological variables using Mann-Kendall and
697 Sen's slope estimator statistical tests in Serbia, *Global and Planetary Change*, 100, 172-182,
698 10.1016/j.gloplacha.2012.10.014, 2013.

699 Gulbeyaz, O., Bond-Lamberty, B., Akyurek, Z., and West, T. O.: A new approach to evaluate the MODIS
700 annual NPP product (MOD17A3) using forest field data from Turkey, *Int J Remote Sens*, 39, 2560-
701 2578, 10.1080/01431161.2018.1430913, 2018.

702 Haberl, H., Erb, K. H., and Krausmann, F.: Human Appropriation of Net Primary Production: Patterns,
703 Trends, and Planetary Boundaries, *Annu Rev Env Resour*, 39, 363-391, 10.1146/annurev-environ-
704 121912-094620, 2014.

705 Harper, A. B., Wiltshire, A. J., Cox, P. M., Friedlingstein, P., Jones, C. D., Mercado, L. M., Sitch, S.,
706 Williams, K., and Duran-Rojas, C.: Vegetation distribution and terrestrial carbon cycle in a carbon
707 cycle configuration of JULES4.6 with new plant functional types, *Geosci Model Dev*, 11, 2857-
708 2873, 10.5194/gmd-11-2857-2018, 2018.

709 Harris, I., Osborn, T. J., Jones, P., and Lister, D.: Version 4 of the CRU TS monthly high-resolution
710 gridded multivariate climate dataset, *Scientific Data*, 7, 109, 10.1038/s41597-020-0453-3, 2020.

711 Hovenden, M. J., Newton, P. C., and Wills, K. E.: Seasonal not annual rainfall determines grassland
712 biomass response to carbon dioxide, *Nature*, 511, 583-586, 10.1038/nature13281, 2014.

713 Humphrey, V., Zscheischler, J., Ciais, P., Gudmundsson, L., Sitch, S., and Seneviratne, S. I.: Sensitivity
714 of atmospheric CO₂ growth rate to observed changes in terrestrial water storage, *Nature*, 560, 628-
715 631, 10.1038/s41586-018-0424-4, 2018.

716 Humphrey, V., Berg, A., Ciais, P., Gentine, P., Jung, M., Reichstein, M., Seneviratne, S. I., and
717 Frankenberg, C.: Soil moisture–atmosphere feedback dominates land carbon uptake variability,
718 *Nature*, 592, 65-69, 10.1038/s41586-021-03325-5, 2021.

719 Hurtt, G. C., Chini, L. P., Frolking, S., Betts, R. A., Feddema, J., Fischer, G., Fisk, J. P., Hibbard, K.,
720 Houghton, R. A., Janetos, A., Jones, C. D., Kindermann, G., Kinoshita, T., Goldewijk, K. K., Riahi,
721 K., Shevliakova, E., Smith, S., Stehfest, E., Thomson, A., Thornton, P., van Vuuren, D. P., and
722 Wang, Y. P.: Harmonization of land-use scenarios for the period 1500-2100: 600 years of global
723 gridded annual land-use transitions, wood harvest, and resulting secondary lands, *Climate Change*,
724 109, 117-161, 10.1007/s10584-011-0153-2, 2011.

725 Hurtt, G. C., Chini, L., Sahajpal, R., Frolking, S., Bodirsky, B. L., Calvin, K., Doelman, J. C., Fisk, J.,

726 Fujimori, S., Goldewijk, K. K., Hasegawa, T., Havlik, P., Heinemann, A., Humpenöder, F.,
727 Jungclauss, J., Jed Kaplan, Kennedy, J., Kristzin, T., Lawrence, D., Lawrence, P., Ma, L., Mertz, O.,
728 Pongratz, J., Popp, A., Poulter, B., Riahi, K., Shevliakova, E., Stehfest, E., Thornton, P., Tubiello,
729 F. N., van Vuuren, D. P., Zhang, X.: Harmonization of Global Land-Use Change and Management
730 for the Period 850-2100 (LUH2) for CMIP6, *Geoscientific Model Development*, 13, 5425-5464,
731 10.5194/gmd-13-5425-2020, 2021.

732 IPCC: Impacts, Adaptation and Vulnerability. Contribution of Working Group II to the Fourth
733 Assessment Report of the Intergovernmental Panel on Climate Change, 2007.

734 Jung, M., Reichstein, M., Schwalm, C. R., Huntingford, C., Sitch, S., Ahlstrom, A., Arneeth, A., Camps-
735 Valls, G., Ciais, P., Friedlingstein, P., Gans, F., Ichii, K., Jain, A. K., Kato, E., Papale, D., Poulter,
736 B., Raduly, B., Rodenbeck, C., Tramontana, G., Viovy, N., Wang, Y. P., Weber, U., Zaehle, S., and
737 Zeng, N.: Compensatory water effects link yearly global land CO₂ sink changes to temperature,
738 *Nature*, 541, 516-520, 10.1038/nature20780, 2017.

739 Kaplan, J. O., Krumhardt, K. M., Ellis, E. C., Ruddiman, W. F., Lemmen, C., and Goldewijk, K. K.:
740 Holocene carbon emissions as a result of anthropogenic land cover change, *Holocene*, 21, 775-791,
741 10.1177/0959683610386983, 2011.

742 Keenan, T. F., Prentice, I. C., Canadell, J. G., Williams, C. A., Wang, H., Raupach, M., and Collatz, G.
743 J.: Recent pause in the growth rate of atmospheric CO₂ due to enhanced terrestrial carbon uptake
744 *Nat Commun*, 7, 10.1038/Ncomms16137, 2017.

745 Kindermann, G. E., Mcallum, I., Fritz, S., and Obersteiner, M.: A global forest growing stock, biomass
746 and carbon map based on FAO statistics, *Silva Fenn*, 42, 387-396, 10.14214/Sf.244, 2008.

747 Le Noë, J., Matej, S., Magerl, A., Bhan, M., Erb, K. H., and Gingrich, S.: Modeling and empirical
748 validation of long-term carbon sequestration in forests (France, 1850-2015), *Glob Chang Biol*, 26,
749 2421-2434, 10.1111/gcb.15004, 2020.

750 Liu, J., Bowman, K. W., Schimel, D. S., Parazoo, N. C., Jiang, Z., Lee, M., Bloom, A. A., Wunch, D.,
751 Frankenberg, C., Sun, Y., O'Dell, C. W., Gurney, K. R., Menemenlis, D., Gierach, M., Crisp, D.,
752 and Eldering, A.: Contrasting carbon cycle responses of the tropical continents to the 2015-2016 El
753 Nino, *Science*, 358, eaam5690, 10.1126/science.aam5690, 2017.

754 Ma, H. Z., Mo, L. D., Crowther, T. W., Maynard, D. S., van den Hoogen, J., Stocker, B. D., Terrer, C.,
755 and Zohner, C. M.: The global distribution and environmental drivers of aboveground versus
756 belowground plant biomass, *Nat Ecol Evol*, 5, 1110+, 10.1038/s41559-021-01485-1, 2021.

757 Madani, N., Parazoo, N. C., Kimball, J. S., Ballantyne, A. P., Reichle, R. H., Maneta, M., Saatchi, S.,
758 Palmer, P. I., Liu, Z., and Tagesson, T.: Recent Amplified Global Gross Primary Productivity Due
759 to Temperature Increase Is Offset by Reduced Productivity Due to Water Constraints, *AGU*
760 *Advances*, 2, e2020AV000180, 10.1029/2020AV000180, 2020.

761 Magerl, A., Le Noë, J., Erb, K.-H., Bhan, M., and Gingrich, S.: A comprehensive data-based assessment
762 of forest ecosystem carbon stocks in the U.S. 1907–2012, *Environ Res Lett*, 14, 125015,
763 10.1088/1748-9326/ab5cb6, 2019.

764 McConnaughay, K. D. M. and Coleman, J. S.: Biomass allocation in plants: ontogeny or optimality? A
765 test along three resource gradients, *Ecology*, 80, 2581-2593, 10.1890/0012-
766 9658(1999)080[2581:BAIPOO]2.0.CO;2, 1999.

767 Monteith, J. L. and Unsworth, M. H.: *Principles of Environmental Physics*, 2nd ed., London 1990.

768 Olson, J., Watts, J., and Allison, L.: *Carbon in Live Vegetation of Major World Ecosystems*, Oak Ridge
769 National Laboratory 1983.

770 Pan, Y. D., Birdsey, R. A., Phillips, O. L., and Jackson, R. B.: The Structure, Distribution, and Biomass
771 of the World's Forests, *Annu Rev Ecol Evol S*, 44, 593-622, 10.1146/annurev-ecolsys-110512-
772 135914, 2013.

773 Pan, Y. D., Birdsey, R. A., Fang, J. Y., Houghton, R., Kauppi, P. E., Kurz, W. A., Phillips, O. L.,
774 Shvidenko, A., Lewis, S. L., Canadell, J. G., Ciais, P., Jackson, R. B., Pacala, S. W., McGuire, A.
775 D., Piao, S. L., Rautiainen, A., Sitch, S., and Hayes, D.: A Large and Persistent Carbon Sink in the
776 World's Forests, *Science*, 333, 988-993, 10.1126/science.1201609, 2011.

777 Piao, S. L., Friedlingstein, P., Ciais, P., Zhou, L. M., and Chen, A. P.: Effect of climate and CO₂ changes
778 on the greening of the Northern Hemisphere over the past two decades, *Geophys Res Lett*, 33,
779 L23402, 10.1029/2006GL028205, 2006.

780 Piao, S. L., Wang, X., Wang, K., Li, X., Bastos, A., Canadell, J. G., Ciais, P., Friedlingstein, P., and
781 Sitch, S.: Interannual variation of terrestrial carbon cycle: Issues and perspectives, *Glob Chang Biol*,
782 26, 300-318, 10.1111/gcb.14884, 2020.

783 Poorter, H.: Construction costs and payback time of biomass: a whole plant perspective, *A Whole-Plant
784 Perspective on Carbon-Nitrogen Interactions*, SPB Academic Publishing, The Hague 1994.

785 Poulter, B., Frank, D., Ciais, P., Myneni, R. B., Andela, N., Bi, J., Broquet, G., Canadell, J. G., Chevallier,
786 F., Liu, Y. Y., Running, S. W., Sitch, S., and van der Werf, G. R.: Contribution of semi-arid
787 ecosystems to interannual variability of the global carbon cycle, *Nature*, 509, 600-603,
788 10.1038/nature13376, 2014.

789 Prentice, I. C., Harrison, S. P., and Bartlein, P. J.: Global vegetation and terrestrial carbon cycle changes
790 after the last ice age, *New Phytol*, 189, 988-998, 10.1111/j.1469-8137.2010.03620.x, 2011.

791 Roy, J., Saugier, B., and Mooney, H. A.: Estimations of global terrestrial productivity: converging toward
792 a single number? In: *Terrestrial Global Productivity*, Academic Press, San Diego 2001.

793 Ruesch, A. and Gibbs, H. K.: New IPCC Tier-1 global biomass carbon map for the year 2000, 2008.

794 Ryan, M. G.: Effects of Climate Change on Plant Respiration, *Ecological Applications*, 1, 157-167,
795 10.2307/1941808, 1991.

796 Sato, H., Itoh, A., and Kohyama, T.: SEIB-DGVM: A new Dynamic Global Vegetation Model using a
797 spatially explicit individual-based approach, *Ecological Modelling*, 200, 279-307,
798 10.1016/j.ecolmodel.2006.09.006, 2007.

799 Sato, H., Kobayashi, H., Beer, C., and Fedorov, A.: Simulating interactions between topography,
800 permafrost, and vegetation in Siberian larch forest, *Environ Res Lett*, 15, 095006, 10.1088/1748-
801 9326/Ab9be4, 2020.

802 Saugier, B., Roy, J., and Mooney, H.: Estimations of Global Terrestrial Productivity, *Terrestrial Global
803 Productivity*, Academic Press, San Diego, Calif 2001.

804 Schimel, D., Stephens, B. B., and Fisher, J. B.: Effect of increasing CO₂ on the terrestrial carbon cycle,
805 *Proceedings of the National Academy of Sciences of the United States of America*, 112, 436-441,
806 10.1073/pnas.1407302112, 2015.

807 Seo, H. and Kim, Y.: Interactive impacts of fire and vegetation dynamics on global carbon and water
808 budget using Community Land Model version 4.5, *Geosci Model Dev*, 12, 457-472, 10.5194/gmd-
809 12-457-2019, 2019.

810 Shevliakova, E., Pacala, S. W., Malyshev, S., Hurtt, G. C., Milly, P. C. D., Caspersen, J. P., Sentman, L.
811 T., Fisk, J. P., Wirth, C., and Crevoisier, C.: Carbon cycling under 300 years of land use change:
812 Importance of the secondary vegetation sink, *Global Biogeochem Cy*, 23, 10.1029/2007gb003176,
813 2009.

814 Sun, F., Roderick, M. L., and Farquhar, G. D.: Changes in the variability of global land precipitation,
815 *Geophys Res Lett*, 39, L19402, 10.1029/2012gl053369, 2012.

816 Tei, S., Sugimoto, A., Liang, M. C., Yonenobu, H., Matsuura, Y., Osawa, A., Sato, H., Fujinuma, J., and
817 Maximov, T.: Radial Growth and Physiological Response of Coniferous Trees to Arctic
818 Amplification, *J Geophys Res-Bioge*, 122, 2786-2803, 10.1002/2016JG003745, 2017.

819 Terrer, C., Phillips, R. P., Hungate, B. A., Rosende, J., Pett-Ridge, J., Craig, M. E., van Groenigen, K. J.,
820 Keenan, T. F., Sulman, B. N., Stocker, B. D., Reich, P. B., Pellegrini, A. F. A., Pendall, E., Zhang,
821 H., Evans, R. D., Carrillo, Y., Fisher, J. B., Van Sundert, K., Vicca, S., and Jackson, R. B.: A trade-
822 off between plant and soil carbon storage under elevated CO₂, *Nature*, 591, 599-603,
823 10.1038/s41586-021-03306-8, 2021.

824 Tharammal, T., Bala, G., Devaraju, N., and Nemani, R.: A review of the major drivers of the terrestrial
825 carbon uptake: model-based assessments, consensus, and uncertainties, *Environ Res Lett*, 14,
826 093005, 10.1088/1748-9326/Ab3012, 2019.

827 Tong, X. W., Brandt, M., Yue, Y. M., Ciais, P., Jepsen, M. R., Penuelas, J., Wigneron, J. P., Xiao, X.
828 M., Song, X. P., Horion, S., Rasmussen, K., Saatchi, S., Fan, L., Wang, K. L., Zhang, B., Chen, Z.
829 C., Wang, Y. H., Li, X. J., and Fensholt, R.: Forest management in southern China generates short
830 term extensive carbon sequestration, *Nat Commun*, 11, 10.1038/s41467-019-13798-8, 2020.

831 West, P. C., Gibbs, H. K., Monfreda, C., Wagner, J., Barford, C. C., Carpenter, S. R., and Foley, J. A.:
832 Trading carbon for food: Global comparison of carbon stocks vs. crop yields on agricultural land,
833 *Proceedings of the National Academy of Sciences of the United States of America*, 107, 19645-
834 19648, 10.1073/pnas.1011078107, 2010.

835 Wild, M., Gilgen, H., Roesch, A., Ohmura, A., Long, C. N., Dutton, E. G., Forgan, B., Kallis, A., Russak,
836 V., and Tsvetkov, A.: From dimming to brightening: Decadal changes in solar radiation at Earth's
837 surface, *Science*, 308, 847-850, 10.1126/science.1103215, 2005.

838 Yang, Y., Fang, J., Ma, W., Guo, D., and Mohammat, A.: Large-scale pattern of biomass partitioning
839 across China's grasslands, *Global Ecology and Biogeography*, 19, 268-277, 10.1111/j.1466-
840 8238.2009.00502.x, 2010.

841 Zhang, H., Song, T. Q., Wang, K. L., Yang, H., Yue, Y. M., Zeng, Z. X., Peng, W. X., and Zeng, F. P.:
842 Influences of stand characteristics and environmental factors on forest biomass and root-shoot
843 allocation in southwest China, *Ecol Eng*, 91, 7-15, 10.1016/j.ecoleng.2016.01.040, 2016.

844 Zhu, Z. C., Piao, S. L., Myneni, R. B., Huang, M. T., Zeng, Z. Z., Canadell, J. G., Ciais, P., Sitch, S.,
845 Friedlingstein, P., Arneeth, A., Cao, C. X., Cheng, L., Kato, E., Koven, C., Li, Y., Lian, X., Liu, Y.
846 W., Liu, R. G., Mao, J. F., Pan, Y. Z., Peng, S. S., Penuelas, J., Poulter, B., Pugh, T. A. M., Stocker,
847 B. D., Viovy, N., Wang, X. H., Wang, Y. P., Xiao, Z. Q., Yang, H., Zaehle, S., and Zeng, N.:
848 Greening of the Earth and its drivers, *Nat Clim Change*, 6, 791-+, 10.1038/Nclimate3004, 2016.